BAND PASS FILTERS FOR DETERMINING SHOCK LOCATIONS*

ROBERT BRUCE BAUER †

Abstract. Gibbs demonstrated that truncating a Fourier representation of a discontinuous function produces a highly oscillatory function. New techniques can now obtain exponentially accurate expansions from a truncated Fourier representation. But many of these techniques require accurate knowledge of the shock locations. The Prony method provides such an estimation, but this method requires an a priori knowledge of the number of shocks. The method presented here will not need to know how many shocks exist, and still provide an accurate estimation of the shock location. Another concern was to make this method find the shock locations with the same accuracy whether or not there are contact discontinuities (discontinuities in the derivatives) in the data.

Key words. Spectral Methods, Shock Location, Filtering

AMS subject classifications. 42a16, 42–04, 65T10, 65–04

1. Introduction. Edge detection has been a problem of great interest in the field of pattern recognition for many years. The problem is basic in the reconstruction of 3-dimensional objects from 2-dimensional pictures. Marr [12], Witkin [19] and Rosenfeld and Thurston [14] have all used some type of filtering to detect edges. These methods looked for a zero crossing of a filtered function. Stephan Mallat has headed up research into using wavelets to detect edges and has had very encouraging results. [15]

Within the confines of numerical analysis, the problem of edge detection has taken on a new importance. Numerical procedures are now being developed to solve problems with discontinuous solutions. One area of continual research is how to post-process the output from a numerical scheme. Gottlieb et. al. have developed a method to reconstruct discontinuous functions given the truncated Fourier coefficients of that function [8]. The other information required to preform this reconstruction is the location of the shock locations. If the shock locations are known, a spectrally accurate reconstruction of the original function can be computed using Gegenbauer polynomials.

The method within this paper was designed to provide that information precisely. Given the Fourier coefficients of a discontinuous function, this method computes the location of the discontinuities. Another attempt to locate shocks given Fourier coefficients is the work of Knut Eckhoff [5] [6]. Eckhoff's method constructs a set of non–linear equations for the shock locations and the amplitudes of the jumps.

A background of Fourier Transforms, filtering, wavelets, and some important functions is given later in this section. This is followed by some examples which provide motivation why filtering

*Research supported by AFOSR grant 93-1-0090, DARPA grant N00014-91-4016 and NSF grant DMS-92-11820.

† Center for Applied Mathematical Sciences, USC, Los Angeles, CA 90089-1113, e-mail: rbbauer@cams.usc.edu

will accomplish the desired task. Section 3 examines the behavior of important functions which are integral to showing that the method will find the shock locations. This is followed by descriptions of two algorithms for determining shock locations. Section 4 describes the Cell Shock Location algorithm which is similar to algorithms in edge detection and relies on finding a zero of a filtered discontinuous function. The algorithm will give similar results, but is specifically designed for finding shocks given the Fourier coefficients. While these algorithms give estimates of shock locations, they are low order estimates with errors slightly smaller than the distance between grid points. Section 5 finds Sub-Cell filters which give a highly accurate estimate of the shock location. These filters require a general estimate of shock locations, before they can be used. Therefore, they need the information from the Cell Shock algorithm. In combination, these two algorithms give highly accurate estimates of shock locations given the truncated Fourier coefficients of the function.

1.1. Continuous Fourier Transform. Given a function $f(x)$ defined on $[0, 2\pi)$ such that $\int_0^{2\pi} |f(x)| dx < \infty$, then the continuous Fourier transform is defined as

$$\hat{f}_k = \frac{1}{2\pi}\int_0^{2\pi} f(x)\, e^{-\imath kx} dx. \tag{1.1}$$

Also define a new function $\bar{f}(x)$ as

$$\bar{f}(x) = \sum_{k=-\infty}^{\infty} \hat{f}_k\, e^{\imath kx}. \tag{1.2}$$

It is well known that

$$\bar{f}(x) = \frac{1}{2}\left[f(x^+) + f(x^-)\right]. \tag{1.3}$$

Now define the set of functions which will make up the function space:

$$\mathcal{B}_N = \text{span}\left\{\cos(jx), \sin(kx) \mid j = 0 \ldots N, k = 1 \ldots N\right\}. \tag{1.4}$$

Define the projection operator P_N onto the space $\mathcal{B}_N$ as

$$f_N(x) = P_N f(x) = \sum_{k=-N}^{N} \hat{f}_k\, e^{\imath kx}. \tag{1.5}$$

The projection P_N produces a truncated Fourier series.

1.1.1. Accuracy of a Truncated Fourier Representation. Given a 2π–periodic function $f(x) \in \mathcal{C}^{m-1}$, with $f^{(m)}(x)$ piecewise continuous and

$$\int_0^{2\pi} \left(f^{(m+1)}(x)\right)^2 dx < \infty, \tag{1.6}$$

then the Fourier Coefficients [7] behave like

$$\hat{f}_k = \mathcal{O}\left(\frac{1}{\mid k\mid^{m+1}}\right) \quad \text{as} \quad k \to \pm\infty. \tag{1.7}$$

Furthermore, the associated error from truncating the Fourier series is

$$\max_{0\leq x\leq 2\pi} \mid P_N f(x) - f(x) \mid = \mathcal{O}\left(\frac{1}{N^m}\right) \quad \text{as} \quad N \to \infty. \tag{1.8}$$

For any x away from a discontinuity

$$\mid P_N f(x) - f(x) \mid = \mathcal{O}\left(\frac{1}{N^{m+1}}\right) \quad \text{as} \quad N \to \infty. \tag{1.9}$$

While continuous analytic functions led to exponentially decreasing error bounds, this paper studies discontinuous functions. Therefore $m = 0$ and the maximum norm of the error doesn't decay. Figure 1.1 shows the accuracy problems of representing a discontinuous function by a truncated Fourier series. The unmistakable oscillations which are largest near the discontinuity and slowly diminish are the well know Gibbs Phenomenon.

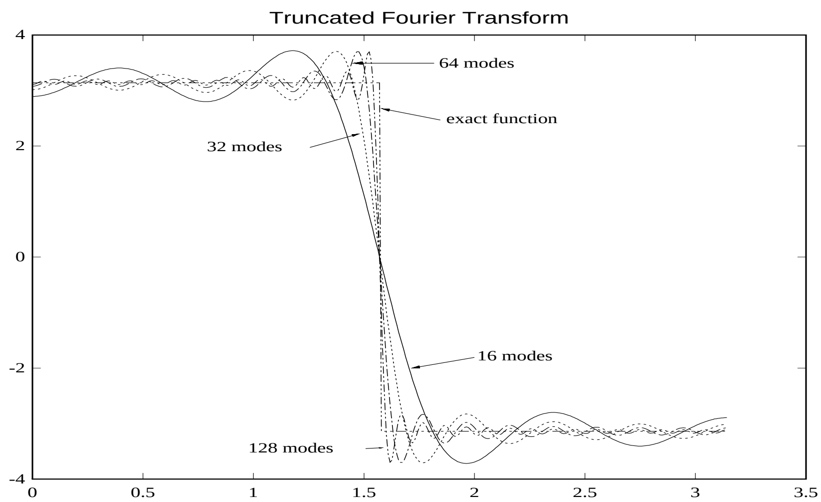

Fig. 1.1: Example of Gibbs Phenomenon: Heavyside function located at $x = \pi/2$. The resulting Fourier Transform was truncated at 16,32,64 & 128 modes.

1.2. Representation of Discontinuities. These three functions will show continued importance throughout this section.

$$a(x) = \begin{cases} \frac{x-\pi}{2\pi} & \text{if } x \in [0, 2\pi) \\ a(x \; mod \, 2\pi) & \text{otherwise} \end{cases} \tag{1.10a}$$

$$b(x) = \begin{cases} \frac{x^2}{4\pi} - \frac{x}{2} + \frac{\pi}{6} & \text{if } x \in [0, 2\pi) \\ b(x \; mod \, 2\pi) & \text{otherwise} \end{cases} \tag{1.10b}$$

$$c(x) = \begin{cases} \frac{x^3}{12\pi} - \frac{x^2}{4} + \frac{\pi x}{6} & \text{if } x \in [0, 2\pi) \\ c(x \; mod \, 2\pi) & \text{otherwise} \end{cases} \tag{1.10c}$$

The first contains a single discontinuity of the function. The second and third functions contain a discontinuity in either the first or second derivative. These functions are also the first three Bernoulli polynomials [2]. These functions, $a(x)$, $b(x)$, and $c(x)$, are going to be used to break down functions into four parts; jumps in functional value, jumps in 1^{st} derivative, jumps in 2^{nd} derivative, and jumps in all other derivatives.

LEMMA 1.1. *Let $f(x)$ be a 2π periodic function with $P+1$ discontinuities in either the function, first derivative or second derivative. Let $\{\xi_0 \ldots \xi_P\}$ be the $P+1$ points of discontinuity. Define $[f(x)]$ as the jump in the function at the point x,*

$$[f(x)] = f(x^+) - f(x^-). \tag{1.11}$$

Let A_j, B_j, and C_j be the jumps in the functions f, f', f'' at the points x_j respectively.

$$\begin{aligned} A_j &= [f(\xi_j)] \\ B_j &= [f'(\xi_j)] \\ C_j &= [f''(\xi_j)] \end{aligned} \tag{1.12}$$

Then $f(x)$ can be written as translates of $a(x)$, $b(x)$, $c(x)$, and a smooth function $S(x)$,

$$f(x) = \sum_{j=0}^{P} (A_j a(x-\xi_j) + B_j b(x-\xi_j) + C_j c(x-\xi_j)) + S(x) \tag{1.13}$$

where $S(x) \in \mathcal{C}^3$, and

$$\hat{S}_k = \mathcal{O}\left(\frac{1}{k^4}\right) \qquad as \quad k \to \pm\infty. \tag{1.14}$$

Proof. To show that $S(x) \in \mathcal{C}^3$ and equation (1.14) holds. Given $f(x)$, the $P+1$ points of discontinuity and the amplitudes of the jumps in the function, first derivative and second derivative, define $\mathcal{F}(x)$ as

$$\mathcal{F}(x) = \sum_{j=0}^{P} (A_j a(x-\xi_j) + B_j b(x-\xi_j) + C_j c(x-\xi_j)). \tag{1.15}$$

Also define $S(x)$ as

$$S(x) = f(x) - \mathcal{F}(x). \tag{1.16}$$

It is clear that $f(x)$ and $\mathcal{F}(x)$ have the same discontinuities in the function, first derivative and second derivative, along with amplitude at these discontinuities. Therefore their difference will be void of any discontinuities in the function, first derivative and second derivative, and therefore $S(x) \in \mathcal{C}^3$. Now using (1.7), it is obvious that

$$\hat{S}_k = \mathcal{O}\left(1/k^4\right). \tag{1.17}$$

□

ASSUMPTION 1. *The only assumption needed is that the jumps in the function to be detected are not too small.*

$$|A_p| = \mathcal{O}(1) \tag{1.18}$$

This requirement ensures that the Gibbs oscillations resulting from a shock are not so small that they tend to blend in with other natural occurrences in the data.

Define the Fourier transforms of $a(x)$, $b(x)$ and $c(x)$ as α_k, β_k, and γ_k,

$$\alpha_k = \frac{-\imath}{2\pi k} \tag{1.19a}$$

$$\beta_k = \frac{-1}{2\pi k^2} \tag{1.19b}$$

$$\gamma_k = \frac{}{2\pi \imath k^3}. \tag{1.19c}$$

1.3. Contact Discontinuity. Given a function $f(x)$, x_0 is a point of contact discontinuity if

$$f(x_0^-) = f(x_0^+) \tag{1.20}$$

and there exists some $p > 0$ such that

$$f^{(p)}(x_0^-) \neq f^{(p)}(x_0^+). \tag{1.21}$$

The strength of the contact discontinuity is the smallest value of p such that equation (1.21) holds.

1.4. Filtering . Filtering a truncated Fourier series has been used to reduce the oscillations due to sharp gradients in the data. Hervé VanDeven [18] showed that if given the Fourier coefficients of a discontinuous function $f(x)$, a low pass filter leads to a better convergence of $f_N^\sigma(x)$ away from the shock. He stated that:

> Let Ω be an open set which contains all the points where $f(x)$ is irregular [points near a discontinuity]. We give some conditions about σ in order that f_N^σ converges uniformly to f in the set $[0, 2\pi] \setminus \Omega$; we show that the rate of this convergence can be exponential. [18]

There are many different filters which will be considered throughout this paper. Because of the numerous filters a strict notation for different filters will be maintained.

$\eta(\omega) \rightarrow$ generic filter

$\sigma(\omega) \rightarrow$ low pass filter

$\mu(\omega) \rightarrow$ band pass filter

$\nu(\omega) \rightarrow$ Sub–Cell Filter

All filters considered within this paper are even filters regardless of which frequencies they allow to pass. Often the expression η_k will be used to represent $\eta(k/N)$.

Filter is a function $\eta : [-1,1] \to R$ which modifies the Fourier coefficients in the following way.

$$f_N^\eta(x) = \sum_{k=-N}^{N} \eta(k/N)\, \hat{f}(k)\, e^{ikx} \tag{1.22}$$

Low pass filter allows the lower frequencies to pass, while attenuating the higher frequencies.

High pass filter is the opposite of a low pass filter in that it attenuates the low frequencies, and allows the higher frequencies to pass. Frequently a high pass filter is defined as $1-\sigma$.

Band pass filter allows middle range frequencies to pass, while attenuating the low and high frequencies. eg:

$$\mu(\omega) = \begin{cases} 0, & \text{for } \mid\omega\mid < .3, \\ 1, & \text{for } .3 \le \mid\omega\mid < .7, \\ 0, & \text{for } .7 \le \mid\omega\mid . \end{cases} \qquad \textit{ideal band pass filter}$$

$$\mu(\omega) = \sin^\rho(\pi\omega) \qquad \textit{sine band pass filter}$$

$$\mu(\omega) = 2^\rho\, \omega^\rho (1-|\omega|)^\rho \qquad \textit{analytic band pass filter}$$

$$\mu(\omega) = e^{-l\omega^\rho} - e^{-h\omega^\rho} \qquad \textit{exponential band pass filter} \qquad l > h$$

Band pass filter of order ρ is a band pass filter, $\mu \in \mathcal{C}^\rho_{[-1,1]}$ with the following properties:

$$\mu^{(j)}(0) = 0 \quad \text{for} \quad j = 0 \ldots (\rho-1) \tag{1.24a}$$

$$\mu^{(j)}(1) = 0 \quad \text{for} \quad j = 0 \ldots (\rho-1)\,. \tag{1.24b}$$

Cut–off: Given a filter function which maps $[0,1] \to [0,1]$, a cut–off value is such that $\sigma(\omega_{cut-off}) = .5$. This is a break point between frequencies which are allow to pass and are cut–off. For a band pass filter there are two cut–off values, ω_{low} and ω_{high}. For a band pass filter this value $\omega_{\text{cut-off}}$, is such that

$$\omega < \omega_{low} \quad \text{or} \quad \omega > \omega_{high} \qquad , \sigma(\omega) < \frac{1}{2}.$$

1.4.1. Specific Filters. For the purposes of the Cell Shock Location algorithm, let $\mu(\omega)$ be a non–negative band pass filter. The algorithm actually compares the results of using different band pass filters with different orders and cut-offs.

The Cell Shock Location uses a sequence of filters and then compares and contrasts the effects of filtering a discontinuous function. Denote the sequence of filters being used as $\mu^1(\omega)$, $\mu^2(\omega)$, $\mu^3(\omega) \ldots \mu^p(\omega)$. Each of these filters will have different orders and cut-offs. Table 1.4.1 gives examples of different sequences of filters.

Filter Sequence #1			Filter Sequence #2		
Order	ω_{low}	ω_{high}	Order	ω_{low}	ω_{high}
3	.3	.55	3	.75	1
3	.55	.7	1	.5	1
1	.2	.3	5	.5	.75
			5	.75	1

1.4.2. Relationship to Wavelets. (Note: Background and specific definitions of wavelets can be found in Appendix A.)

Consider the wavelet expansion (equations (B.2) and (B.5).)

$$f(x) = \sum_n \alpha_{J,n} \phi_n^J(x) + \sum_{m=1}^{M} \sum_n \beta_{m,n}\, \psi_n^m(x) \tag{1.25}$$

$$\alpha_{m,n} = \int f(x)\, \phi_n^m(x)\, dx \tag{1.26}$$

$$\beta_{m,n} = \int f(x)\, \psi_n^m(x)\, dx \tag{1.27}$$

The coefficients $\alpha_{J,n}$ and $\beta_{m,n}$ contain information on different frequencies. It is known that $\hat{\psi}(\omega)$ is a high pass filter. Then $\widehat{\psi^m}(\omega)$ are also high pass filters which allow a different part of the spectrum through. Consider the Haar wavelet:

$$\psi_0^j(x) = \begin{cases} 1 & \text{for } x \in [0, .5^{j+1}] \\ -1 & \text{for } x \in [.5^{j+1}, .5^j] \\ 0 & \text{for } x \notin [0, .5^j] \end{cases} . \tag{1.28}$$

Their transforms are:

$$\widehat{\psi^j}(\omega) = \frac{(1 - e^{\imath\omega/2^j})^2}{\imath\omega} \tag{1.29}$$

and they are either a band pass or possibly a high pass filter depending on the value of j. Using these filters results in a slightly similar process. The filters are no longer purely real. The most striking difference will come in the sub-cell filters. These filters will give exceptionally accurate estimates of the shock location while wavelets can only estimate within a grid point.

1.5. Effects of filtering. Recall that in figure 1.1 the truncated Fourier representation of a step function lead to some large oscillations around the jump. The benefits of filtering the Fourier coefficients with a low pass filter are a well known solution for the large oscillations. Figure 1.2 shows the result of a fourth order low pass filter on a step function.

From (1.13) in Lemma 1.1 the Fourier Transform of $f(x)$ can be expressed as

$$\hat{f}_k = \sum_{j=0}^{P} e^{\imath k \xi_j} \left(A_j\, \alpha_k + B_j\, \beta_k + C_j\, \gamma_k\right) + \hat{S}_k . \tag{1.30}$$

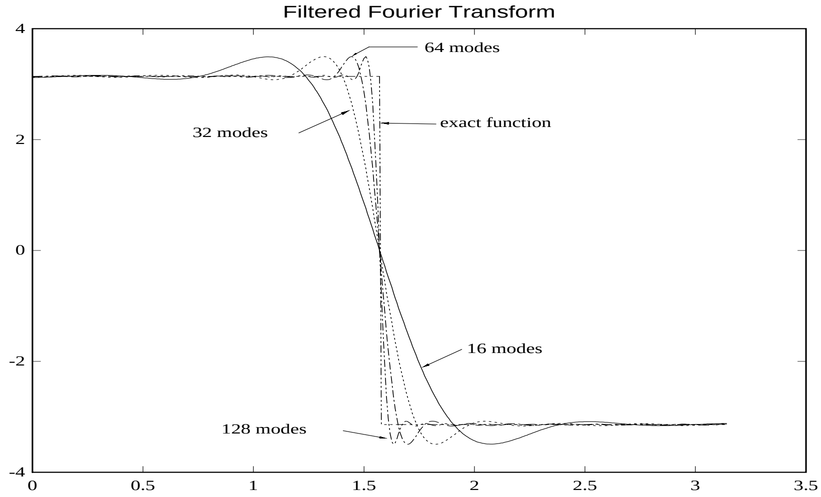

Fig. 1.2: Result of applying a fourth order low pass filter to the truncated Fourier coefficients of a Heavyside step function.

The effect of filtering $a_N(x)$, $b_N(x)$ and $c_N(x)$ will be used in finding the effect of filtering the previous equation.

$$a_N^\eta(x) = -2\sum_{k=1}^{N}\left(\frac{\eta_k}{k}\right)\ \sin(kx) \tag{1.31}$$

$$b_N^\eta(x) = 2\sum_{j=1}^{N}\left(\frac{\eta_k}{k^2}\right)\ \cos(kx) \tag{1.32}$$

$$c_N^\eta(x) = 2\sum_{j=1}^{N}\left(\frac{\eta_k}{k^3}\right)\ \sin(kx) \tag{1.33}$$

Then the result of filtering $f(x)$ is

$$f_N^\eta(x) = \sum_{j=0}^{P}[A_j\ a_N^\eta(x-\xi_j) + B_j\ b_N^\eta(x-\xi_j) + C_j\ c_N^\eta(x-\xi_j)] + S_N^\eta(x). \tag{1.34}$$

1.5.1. Normalization of filters. The goal of using multiple filters is to check and see where they are similar, and where they differ. Consider using $\eta_1(\omega) = \sin(\pi\omega)$ and $\eta_{100}(\omega) = 100\sin(\pi\omega)$ as filters, and applying them to the Heavyside function $H(x)$ to find the shock located at $x = 0$. To find shocks one looks at similarities between $a_N^{\eta_1}(x)$ and $a_N^{\eta_{100}}(x)$. Since $a_N^{\eta_1}(x)$ might appear as noise compared to $a_N^{\eta_{100}}(x)$, the filters need to be normalized. To consider how to normalize, the important traits of $a_N^\eta(x)$ must be identified. The traits required to locate shocks are the size and location of minimas and maximas and the location of the zeroes of $f_N^\eta(x)$. So that the minimas and maximas are approximately the same magnitude regardless of the filter chosen, normalize by a consistent value of $a_N^\eta(x)$.

Normalization Constant for Filters . The Normalization Constant, Π, of a filter, η, is

$$\Pi(\eta) = \sum_{k=1}^{N} \frac{\eta_k}{k} \sin(\frac{\pi k}{N}) = a_N^{\eta}(\pi/N)/2. \tag{1.35}$$

And re–define η as

$$\eta(\omega) = \frac{1}{\Pi(\eta)}\eta(\omega) \tag{1.36}$$

2. Motivation . This section is designed to present the my thoughts behind this method, with the goal of providing a good understanding of the technique. From equations (1.8) and (1.9) it is known that a truncated Fourier series will provide a poor representation of a discontinuous function. But VanDeven showed that low pass filtering of a truncated Fourier series can provide a better estimate of the function away from any discontinuity [18, Pages 18–19, Lemma III.7]. Alternatively, consider the difference between the original function and a low–pass filtered function. Let $\sigma_1(\omega)$ and $\sigma_2(\omega)$ be two low–pass filters of order ρ. VanDeven showed that

$$|a_N^{\sigma}(x) - a(x)| \leq \mathcal{C}\ N^{1-\rho}\ ||\sigma^{(\rho)}||_{L^2(0,1)}\ x^{-\rho} \tag{2.1}$$

where $\mathcal{C}$ is independent of N, ρ, σ, x. Then taking the difference between $a_N^{\sigma_1}(x)$ and $a_N^{\sigma_2}(x)$ results in

$$|a_N^{\sigma_1}(x) - a_N^{\sigma_2}(x)| \leq 2\mathcal{C}\ N^{1-\rho}\ ||\sigma_1^{(\rho)} - \sigma_2^{(\rho)}||_{L^2(0,1)}\ x^{-\rho}. \tag{2.2}$$

Define $\mu(\omega) = \sigma_1(\omega) - \sigma_2(\omega)$, then $\mu(\omega)$ is a band pass filter and

$$|a_N^{\mu}(x)| < \mathcal{C}\ N^{1-\rho}\ ||\mu^{(\rho)}||_{L^2(0,1)}\ x^{-\rho}. \tag{2.3}$$

Therefore it is expected that $a_N^{\mu}(x)$ will be large around $x = 0$ and decay quickly away from $x = 0$. Figure 2.1 shows the resulting difference. Note that in figure 2.1 each band pass filtered function has a maxima immediately before the shock and a minima following the shock.

A more important trait is that the filtered function is close to zero at the shock location. This trait will be the basis for the Cell Shock Location and is similar to the zero crossing methods[12, 19, 14]. In the first example to follow, the filtered function is exactly equal to zero at the shock location. In the second and third examples, the filtered function is not exactly equal to zero at the shock location. The second two examples do give insight into two requirements on the filter μ. The goal is to find a Sub–Cell Shock filter which will have $f_N^{\mu}(x) \approx 0$ at shock locations.

2.1. Single Sawtooth Function. (Example #1) Consider the function $a(x) = A\ x - \pi$. The Fourier coefficients of $f(x)$ are

$$\hat{f_N}(k) = A\ \alpha_k. \tag{2.4}$$

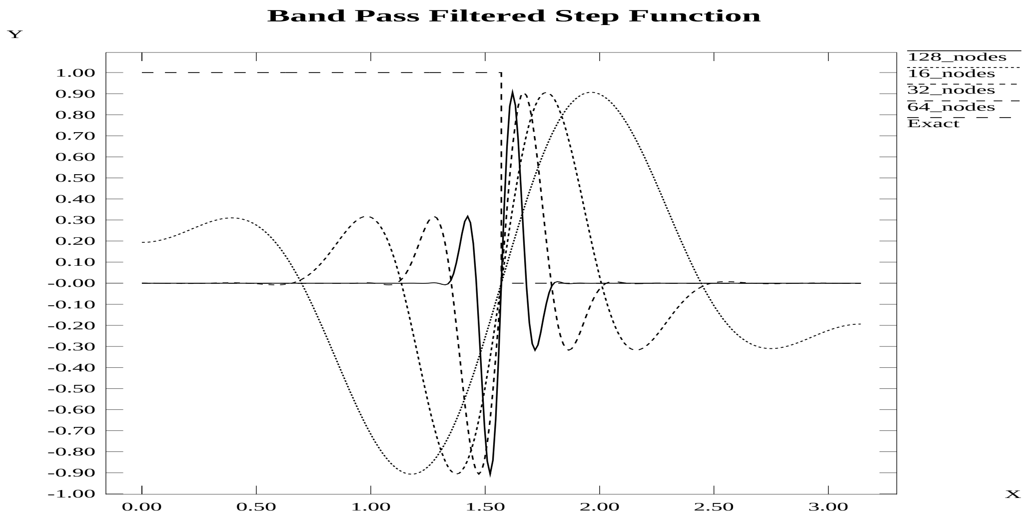

Fig. 2.1: Result of applying a fourth order band pass filter to the truncated Fourier coefficients of a Heavyside step function.

Applying an even filter $\mu(\omega)$ to these Fourier Coefficients

$$\hat{f_N^{\mu}}(k) = A\ \alpha_k\ \mu(k/N). \tag{2.5}$$

results in the following function in the physical space:

$$f_N^{\mu}(x) = 2A\ \sum_{k=1}^{N} \frac{\mu_k}{k}\ \sin(kx) \tag{2.6}$$

Since $\sin(k \cdot 0) = 0$ for all k, $f_N^{\mu}(0) = 0$. Therefore if μ is an even filter and ξ is the location of a single shock, then $f_N^{\mu}(\xi) = 0$.

In figure 2.1, the results of filtering with a band pass filter a step function is shown. Besides having $f_N^{\mu}(0) = 0$, notice the minima and maxima around the shock locations. This minima and maxima will become the basis for the Cell Shock Location.

2.2. Second Example. Consider the function with a discontinuity of size A and a discontinuity in the first and second derivatives of sizes B and C, with all other derivatives identically equal to zero. (All discontinuities are located at $x = 0$.) Then the Fourier transform is

$$\hat{f_N}(k) = A\ \alpha_k + B\ \beta_k + C\ \gamma_k \tag{2.7}$$

which results in the following function in the physical space.

$$f_N^{\mu}(x) = 2A\ \sum_{k=1}^{N} \frac{\mu_k}{k}\ \sin(kx) + 2B\ \sum_{k=1}^{N} \frac{\mu_k}{k^2}\ \cos(kx) \tag{2.8a}$$

$$+\,2C\sum_{k=1}^{N}\frac{\mu_k}{k^3}\sin(kx) \tag{2.8b}$$

$$= A\,a_N^{\mu}(x) + B\,b_N^{\mu}(x) + C\,c_N^{\mu}(x) \tag{2.8c}$$

$$f_N^{\mu}(0) = A\cdot 0 + Bb_N^{\mu}(0) + C\cdot 0 \neq 0 \tag{2.9}$$

If the filters are defined such that $\sum_k \mu_k\cdot\beta_k \approx 0$, then $b_N^{\mu}(0)\approx 0$, and $f_N^{\mu}(0)\approx 0$.

2.2.1. Negative Filters. The previous example leads to a requirement that

$$\sum \beta_k\cdot\mu_k = 0 \tag{2.10}$$

in order for $f_N^{\mu}(x) = 0$ at the shock location. This is not possible if the filter chosen is non-negative. When finding the special Sub-Cell Filter, for which a highly accurate estimate of the shock location is found, this requirement will be dropped.

Define the filter ν_k as

$$\nu_k = \begin{cases} 0 & \text{for } |k/N| < .5 \\ -c\,(3-4k/N)\,\beta_{N(\frac{3}{2}-\frac{k}{N})} & \text{for } .5 \le |k/N| < .75 \\ c\,(4k/N-3)\,\beta_{N(\frac{3}{2}-\frac{k}{N})} & \text{for } .75 \le |k/N| \le 1 \end{cases} \tag{2.11}$$

where $c:[0,1]\to\mathcal{R}^+$ and

$$c(0) = 0, \qquad c(1) = 0, \tag{2.12a}$$

$$c'(0) = 1, \qquad c'(1) = 0, \tag{2.12b}$$

$$c^{(p)}(0) = 0, \qquad c^{(p)}(1) = 0, \tag{2.12c}$$

for $p = 2\ldots\rho$. This filter is similar to a high or band pass filter in that it attenuates the low frequencies. But this filter is negative for several values of k. The benefit of defining this filter is that now

$$\sum_{k=1}^{N}\beta_k\cdot\nu_k = 0 \tag{2.13}$$

and $f_N^{\nu}(0) = 0$.

2.3. Two Sawtooth functions. (Example # 3) Now consider the problem of multiple shocks, and how to minimize the interaction between them. Consider two sawtooth functions of amplitude A_1 and A_2 at locations ξ_1 and ξ_2. The Fourier Transform of this function is

$$\hat{f_N}(k) = \left(A_1\,e^{ik\xi_1} + A_2\,e^{ik\xi_2}\right)\,\alpha_k. \tag{2.14}$$

The filtered Fourier coefficients produce the following function in the physical space

$$f_N^\mu(x) = 2\sum_{k=1}^{N} \frac{\mu_k}{k}\left(A_1 \sin(x-\xi_1) + A_2 \sin(x-\xi_2)\right). \tag{2.15}$$

Which can be re–written as

$$f_N^\mu(x) = A_1\, a_N^\mu(x-\xi_1) + A_2\, a_N^\mu(x-\xi_2). \tag{2.16}$$

Ideally, the zeroes of $f_N^\mu(x)$ should be at ξ_1 and ξ_2. Considering the first shock, evaluate $f_N^\mu(\xi_1)$

$$f_N^\mu(\xi_1) = 0 + A_2\, a_N^\mu(\xi_1-\xi_2). \tag{2.17}$$

Then using the implicit function theorem, the root of $f_N^\mu(x)$ near ξ_1 can be found as,

$$f_N^\mu(\xi_1+\hat{x}) \;= 0 \qquad \hat{x} \doteq -\frac{A_2}{A_1}\frac{a_N^\mu(\xi_1-\xi_2)}{\frac{\partial}{\partial x}a_N^\mu(\xi_1-\xi_2) + \frac{\partial}{\partial x}a_N^\mu(0)}. \tag{2.18}$$

Now if the filter μ is designed such that $a_N^\mu(\xi_1-\xi_2)\approx 0$, then $f_N^\mu(\xi_1)\approx 0$ and this will provide an accurate estimate of the shock location. However, if $a_N^\mu(\xi_1-\xi_2) = \mathcal{O}(1)$, then the estimate will not be accurate.

Each of these three examples have laid the groundwork for the specifications which will become important in defining the filters for this method.

3. Behavior of $\mathbf{a_N^\mu(x)}$, $\mathbf{b_N^\mu(x)}$, $\mathbf{c_N^\mu(x)}$ and $\mathbf{S_N^\mu(x)}$. The size of $S_N^\mu(x)$will be checked first then the relative sizes of $a_N^\mu(x)$, $b_N^\mu(x)$, and $c_N^\mu(x)$ will be compared and it will be shown that $a_N^\mu(x)$ is the dominant feature for $x\in[-2\pi/N, 2\pi/N]$. Now $a_N^\mu(x)$ is dominant in the sense that the size of $a_N^\mu(x)$ is close to constant with respect to N, while $b_N^\mu(x)$and $c_N^\mu(x)$ decay like $1/N$ and $1/N^2$.

Second the size of each function will be seen to be small for x away from zero. The estimates obtained here are used to show that $a_N^\mu(x)$, $b_N^\mu(x)$, and $c_N^\mu(x)$ decay fast enough away from $x=0$, so that multiple shocks can be detected.

LEMMA 3.1. *Let $\mu(\omega)$ be a band pass filter of order ρ. Then for $q>0$,*

$$\sum_{k=1}^{N}\frac{\mu_k}{k^q} = \mathcal{O}(N^{1-min(\rho,q)}) \tag{3.1}$$

or

$$\sum_{k=1}^{N}\frac{\mu_k}{k^q} = \mathcal{K}\, N^{1-min(\rho,q)} + \mathcal{O}\left(N^{-min(\rho,q)}\right) \tag{3.2}$$

where $\mathcal{K}$ is independent of $\mu(\omega)$ and N.

Proof. Using the first order numerical integration formula

$$\frac{1}{N}\sum_{k=1}^{N} f(k/N) \approx \int_0^1 f(x)dx \tag{3.3}$$

and the error estimate for the formula above

$$\left| \int_0^1 f(x)dx - \frac{1}{N}\sum_{k=1}^{N} f(k/N) \right| \leq \frac{1}{2N^2}\sum_{k=1}^{N} M_k \tag{3.4a}$$

$$M_k = \sup_{x\in[(k-1)/N, k/N]} f'(x). \tag{3.4b}$$

Also, if $f'(x)$ is integrable, then

$$\left| \int_0^1 f(x)dx - \frac{1}{N}\sum_{k=1}^{N} f(k/N) \right| \leq \frac{\max_{x\in[0,1]} |f'(x)|}{N}. \tag{3.5}$$

(See [4, 13])

<u>Case 1: $\rho \geq q$</u>

$$\sum_{k=1}^{N} \mu(k/N)/k^q = N^{1-q}\left[\frac{1}{N}\sum_{k=1}^{N}\frac{\mu(k/N)}{(k/N)^q}\right] \tag{3.6a}$$

$$\leq N^{1-q}\int_0^1 \mu(x)/y^q dx + N^{-q}\max_{x\in[0,1]}\left|\frac{d}{dx}\mu(x)/x^q\right| \tag{3.6b}$$

Now since $\mu(\omega)$ is of order $\rho \geq q$ the above integral is bounded and therefore

$$\sum_{k=1}^{N} \mu(k/N)/k^q = \mathcal{O}\left(N^{1-q}\right). \tag{3.7}$$

<u>Case 2: $\rho < q$</u>

$$\sum_{k=1}^{N} \mu(k/N)/k^q = N^{1-\rho}\sum_{k=1}^{N}\frac{1}{k^{q-\rho}}\left[\frac{1}{N}\frac{\mu(k/N)}{(k/N)^\rho}\right] \tag{3.8a}$$

$$\leq N^{1-\rho}\left[\frac{1}{N}\sum_{k=1}^{N}\frac{\mu(K/N)}{(k/N)^\rho}\right] \tag{3.8b}$$

$$\leq N^{1-\rho}\int_0^1 \mu(x)/y^\rho dx + N^{-\rho}\max_{x\in[0,1]}\left|\frac{d}{dx}\mu(x)/x^\rho\right|. \tag{3.8c}$$

Since $\mu(\omega)$ is of order ρ the integral above is bound and therefore

$$\sum_{k=1}^{N} \mu(k/N)/k^q = \mathcal{O}\left(N^{1-\rho}\right). \tag{3.9}$$

□

3.1. Behavior of $\mathbf{S_N^\mu(x)}$. Let $\mu(\omega)$ be a non–negative band pass filter of order greater than or equal to 3. Then

$$S_N^\mu(x) = \sum_{k=-N,N} \mu_k\, \hat{S}_k\, e^{\imath kx}. \tag{3.10}$$

Using $|\hat{S}_k| \le \mathcal{K}/k^4$,

$$|S_N^\mu(x)| \le \sum_{k=-N,N} \left|\mu(k/N)\,\hat{S}_k\right| \left|e^{\imath kx}\right| \tag{3.11a}$$

$$\le \sum_{k=-N}^{N} \left|\mu(k/N)\,\hat{S}_k\right| \tag{3.11b}$$

$$\le 2\mathcal{K} \sum_{k=1}^{N} \frac{\mu(k/N)}{k^4}. \tag{3.11c}$$

Using Lemma 3.1

$$|S_N^\mu(x)| = \mathcal{O}\left(N^{1-\min(\rho,4)}\right). \tag{3.12}$$

3.2. Behavior $\mathbf{a_N^\mu(x)}$, $\mathbf{b_N^\mu(x)}$, and $\mathbf{c_N^\mu(x)}$ near shock. Let $Y_N = [-2\pi/N, 2\pi/N]$. Then for the purposes of describing the behavior of $a_N^\mu(x)$, $b_N^\mu(x)$, and $c_N^\mu(x)$ near a shock, examine the point $X \in Y_N$ where $X \in [-2\pi, 2\pi]$.

The reason for choosing the point X/N and later X_N/N is that observations of $a_N^\mu(x)$ in figure 2.1 show that as N increases the function $a_N^\mu(x)$ is compressed towards the shock. A first estimate of the rate of compression towards the shock is that features move at a rate of $1/N$. Thus the value of $a_N^\mu(X/N)$ should be approximately constant with respect to N for values in Y_N.

$$a_N^\mu(X/N) = \mathcal{O}(1) \tag{3.13a}$$

$$b_N^\mu(X/N) = \mathcal{O}(N^{-1}) \tag{3.13b}$$

$$c_N^\mu(X/N) = \mathcal{O}(N^{-2}) \tag{3.13c}$$

3.2.1. Maximum of $\mathbf{a_N^\mu(x)}$.

LEMMA 3.2. *For a non–negative band pass filter even about the point 1/2, then*

$$\mu(.5+\omega) = \mu(.5-\omega) \tag{3.14}$$

and

$$|a_N^\mu(x)| \le a_N^\mu(\pi/N) \tag{3.15}$$

for all x.

Proof. First, to prove that $a_N^\mu(\pi/N)$ is a local maximum.

$$\frac{d}{dx} a_N^\mu(\pi/N) = \sum_{k=1}^{N} \mu(k/N)\cos(\pi k/N) \tag{3.16}$$

Since $\mu(k/N)$ is even about the point $k = N/2$ and $\cos(\pi k/N)$ is odd about the point $k = N/2$, their sum over $k = 1, N-1$ will be zero. ☐

Now consider the filter which is not necessarily symmetric about the point 1/2, but is a general non–negative band pass filters of order ρ. Let X_N/N be the point at which $a_N^\mu(x)$ reaches a maximum.

The goal is to find a lower bound on $a_N^\mu(X_N/N)$.

$$a_N^\mu(X_N/N) = \sum_{k=1}^{N} \mu(k/N)\,\sin(kX_N/N)/k \tag{3.17a}$$

$$= \frac{1}{N}\sum_{k=1}^{N} \frac{\sin(kX_N/N)\mu(k/N)}{(k/N)} \tag{3.17b}$$

$$\geq \int_0^1 \frac{\mu(x)\,\sin(xX_N)}{x}dx - \mathcal{K}_a/N \tag{3.17c}$$

where

$$\mathcal{K}_a = \max_{x\in[0,1]}\left|\frac{d}{dx}\left(\frac{\mu(x)\sin(xX_N)}{x}\right)\right|. \tag{3.17d}$$

Equations (3.17c) and (3.17d) are a result of using a first order numerical integration approximation.

Therefore for a point X_N/N, $|a_N^\mu(X_N/N)|$ is equal to a constant, minus something that decays like $1/N$. Recall that all filters are normalized by $\Pi(\mu)$ and therefore

$$a_N^\mu(\pi/N) = 1 \text{ and } \max_{x\in Y_N}|a_N^\mu(x)| \geq 1. \tag{3.18}$$

3.2.2. Maximum of $\mathbf{b_N^\mu(x)}$. It is obvious that for a non–negative band pass filter

$$|b_N^\mu(x)| = \left|\sum_{k=1}^{N}\mu(k/N)\cos(kx)/k^2\right| \leq b_N^\mu(0) \tag{3.19}$$

for all x.

That leaves the task of finding a bound on $b_N^\mu(0)$. Like before

$$b_N^\mu(0) = \sum_{k=1}^{N}\mu(k/N)/k^2 \tag{3.20a}$$

$$= \frac{1}{N}\left[\frac{1}{N}\sum_{k=1}^{N}\mu(k/N)/(k/N)^2\right] \tag{3.20b}$$

$$\leq \frac{1}{N}\int_0^1 \mu(x)/x^2dx + \mathcal{K}_b/N^2 \tag{3.20c}$$

where

$$\mathcal{K}_b = \max_{x\in[0,1]}\left|\frac{d}{dx}\left(\mu(x)/x^2\right)\right|. \tag{3.20d}$$

In order for the integral in equation (3.20c) to be finite, $\mu(\omega)$ must be at least a second order band pass filter. This will also ensure that the constant $\mathcal{K}_b$ defined in equation (3.20d) is bounded.

3.2.3. Maximum of $\mathbf{c}_{\mathbf{N}}^{\mu}(\mathbf{x})$. Let Z_N/N be the point where $|c_N^\mu(x)|$ reaches a maximum. Therefore

$$|c_N^\mu(x)| \leq c_N^\mu(Z_N/N). \tag{3.21}$$

Then

$$c_N^\mu(Z_N) = \sum_{k=1}^{N} \mu(k/N)\sin(kZ_N/N)/k^3 \tag{3.22a}$$

$$\leq \sum_{k=1}^{N} \mu(k/N)/k^3 \tag{3.22b}$$

$$\leq \frac{1}{N^2}\left[\frac{1}{N}\sum_{k=1}^{N} \mu(k/N)/(k/N)^3\right] \tag{3.22c}$$

$$\leq \frac{1}{N^2}\int_0^1 \mu(x)/x^3 dx + \mathcal{K}_c/N^3 \tag{3.22d}$$

where

$$\mathcal{K}_c = \max_{x\in[0,1]}\left|\frac{d}{dx}\left(\mu(x)/x^3\right)\right|. \tag{3.22e}$$

In order that the integral in equation (3.22d) be finite, $\mu(\omega)$ must be at least a third order band pass filter. This will also ensure that the constant $\mathcal{K}_c$ defined in equation (3.22e) is bounded.

3.2.4. Summary of behavior near shock. Therefore, for a band pass filter of order $\rho \geq 3$, the maximum values of $a_N^\mu(x)$, $b_N^\mu(x)$, and $c_N^\mu(x)$ behave like

$$\max_{x\in Y_N} |a_N^\mu(x)| = \mathcal{O}(1) \tag{3.23a}$$

$$\max_{x\in Y_N} |b_N^\mu(x)| = \mathcal{O}(N^{-1}) \tag{3.23b}$$

$$\max_{x\in Y_N} |c_N^\mu(x)| = \mathcal{O}(N^{-2}). \tag{3.23c}$$

Now for a single shock around zero, $f(x) = A\ a(x) + B\ b(x) + C\ c(x)$,

$$f_N^\mu(x) = A\ a_N^\mu(x) + B\ \mathcal{O}(N^{-1}) + C\ \mathcal{O}(N^{-2}). \tag{3.24}$$

Furthermore, for $A > 0$ $f_N^\mu(\pi/N)$ is approximately the maximum the function will obtain, and $f_N^\mu(-\pi/N)$ is approximately the minimum the function will obtain.

3.3. Behavior away from shock. The bounds above are desirable because they bound how large each function will be anywhere in the domain. However the bounds are for a fixed x/N. ie. The value of $a_N^\mu(1.23/N)$ remains close to the same for all N and the value of $b_N^\mu(1.23/N)$ decays like $1/N$.

While these estimates are good for fixed values of x/N, it is also important to know how these functions decay in x. Recall the example of section 2.3. For the interaction between two shocks it is important to know how small $a_N^\mu(x)$ gets for x away from zero. It is most important to have a bound on the decay of $a_N^\mu(x)$ since it is already known that $b_N^\mu(x)$ and $c_N^\mu(x)$ will decay with increasing N. This section will obtain bounds on $a_N^\mu(x)$, $b_N^\mu(x)$, and $c_N^\mu(x)$ in terms of functions like x^{-q}.

VanDeven [18, Page 21] proves that for a low–pass filter, σ of degree ρ, the following bound holds

$$\forall x \in]0, 2\pi[, |a_N^\sigma(x) - a(x)| \leq M(\mu,\rho)\, N^{1-\rho}\, \{x^{1-\rho} + (2\pi - x)^{1-\rho}\} \tag{3.25}$$

where $M(\mu, \rho)$ is defined as

$$M(\mu,\rho) = 2\left(1 + 2^{-\rho}\sum_{n=1}^{\infty} n^{-\rho}\right) ||\mu^{(\rho)}||_{L^2(0,1)}. \tag{3.26}$$

Equivalently, for a band pass filter μ of order ρ

$$\forall x \in]0, 2\pi[, |a_N^\mu(x)| \leq 2M(\mu,\rho)\, N^{1-\rho}\, \{x^{1-\rho} + (2\pi - x)^{1-\rho}\}, \tag{3.27}$$

and for $b_N^\mu(x)$ and $c_N^\mu(x)$,

$$\forall x \in]0, 2\pi[, |b_N^\mu(x)| \leq M(\mu,\rho)\, N^{1-\rho}\, \{x^{2-\rho} + (2\pi - x)^{2-\rho}\}, \tag{3.28a}$$

$$\forall x \in]0, 2\pi[, |c_N^\mu(x)| \leq M(\mu,\rho)\, N^{1-\rho}\, \{x^{3-\rho} + (2\pi - x)^{3-\rho}\}. \tag{3.28b}$$

These can be re–written as a function of the filter, $M(\mu, \rho)$, a function of the number of nodes, $N^{1-\rho}$ and a function of x and ρ,

$$|a_N^\mu(x)| \leq M(\mu,\rho)\, N^{1-\rho}\, \mathcal{B}(x, 1-\rho) \tag{3.29a}$$

$$|b_N^\mu(x)| \leq M(\mu,\rho)\, N^{1-\rho}\, \mathcal{B}(x, 2-\rho) \tag{3.29b}$$

$$|c_N^\mu(x)| \leq M(\mu,\rho)\, N^{1-\rho}\, \mathcal{B}(x, 3-\rho) \tag{3.29c}$$

where

$$\mathcal{B}(x,q) = (x^q - (2\pi - x)^q)\,. \tag{3.30}$$

Table 3.1 shows the values of $M(\mu, \rho)$ for class of filters used for the Cell Shock Location. Figure 3.1 shows both the computed value and the VanDeven estimate of $M(\mu, \rho)$.

Now while we have bounds on $a_N^\mu(x)$, $b_N^\mu(x)$, and $c_N^\mu(x)$, it is still important to find the constants involved. In the previous section, it was shown that the dominant feature which remains after filtering came from $a_N^\mu(x)$ for x close to zero. Now it remains to be seen whether $a_N^\mu(x)$, $b_N^\mu(x)$, and $c_N^\mu(x)$ are small enough not to effect the minima and maxima around other shocks. To do this, a minimal distance between shocks which will allow the shocks to be detected will be computed.

Definition 3.1. *Given a $\delta \ll 1$, the distance $\Theta(\delta, \mu, N, \rho)$ is defined such that*

$$\forall x \in (\Theta, 2\pi - \Theta) \quad |a_N^\mu(x)| \leq \delta \tag{3.31a}$$

$$\forall x \in (\Theta, 2\pi - \Theta) \quad |b_N^\mu(x)| \leq \delta \tag{3.31b}$$

$$\forall x \in (\Theta, 2\pi - \Theta) \quad |c_N^\mu(x)| \leq \delta. \tag{3.31c}$$

Constants for Bounds on $\lvert a_N^{\mu}(x)\rvert$ where $\mu(\omega) = \lvert\omega\rvert^{\rho}(1-\lvert\omega\rvert)^{\rho}$				
		VanDeven Estimate	Computed	Ratio
order (ρ)	$\lvert\lvert\mu(\omega)^{(\rho)}\rvert\rvert_{L^2(0,1)}$	$M_{est}(\mu,\rho)$	$M_{comp}(\mu,\rho)$	$M_{comp}(\mu,\rho)/M_{est}(\mu,\rho)$
3	1.45×10^2	3.34×10^2	3.54×10^1	11%
4	2.05×10^3	4.38×10^3	7.76×10^2	18%
5	3.70×10^4	7.64×10^4	1.28×10^4	17%
6	8.18×10^5	1.66×10^6	3.82×10^5	23%
7	2.12×10^7	4.27×10^7	1.08×10^7	25%

Table 3.1: Computed $L^2(0,1)$ norm of $\lvert\lvert\mu(\omega)^{(\rho)}\rvert\rvert$, with $\mu(\omega) = \lvert\omega\rvert^{\rho}(1-\lvert\omega\rvert)^{\rho}$ – the VanDeven Estimate of $M(\mu,\rho)$ – computed value of $M(\mu,\rho)$ – the ratio of the Computed value of $M(\mu,\rho)$ to the VanDeven Estimate.

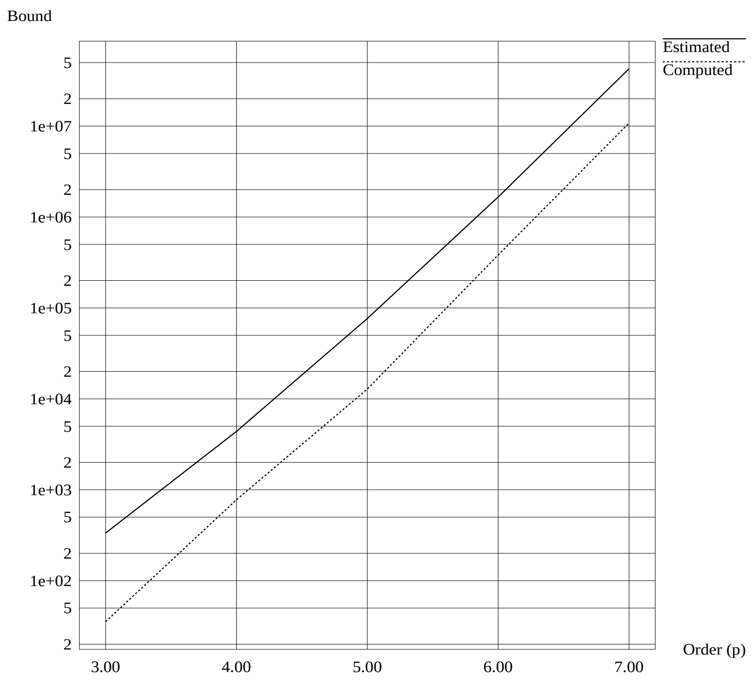

Fig. 3.1: Graphs of VanDeven Estimate of $M(\mu,\rho)$ and the computed value of $M(\mu,\rho)$ for different values of ρ.

This is equivalent to finding $\Theta(\delta,\mu,N,\rho)$ such that

$$\max\left(\mathcal{B}(\Theta,1-\rho),\mathcal{B}(\Theta,2-\rho),\mathcal{B}(\Theta,3-\rho)\right) < \delta\, N^{\rho-1}/M(\mu,\rho). \tag{3.32}$$

N=64			N=128			N=256		
δ	ρ	Θ	δ	ρ	Θ	δ	ρ	Θ
	3	.661		3	.331		3	.165
.01	4	.474	.01	4	.237	.01	4	.118
	5	.224		5	.112		5	.056
	3	.208		3	.104		3	.052
.1	4	.224	.1	4	.112	.1	4	.056
	5	.130		5	.065		5	.032
	3	.161		3	.081		3	.040
.2	4	.177	.2	4	.088	.2	4	.044
	5	.114		5	.057		5	.029

Table 3.2: Computed values of $\Theta(\delta, \mu, N, \rho)$ for different δ, N, ρ. $\mu(\omega) = \omega^{\rho}(1-\omega)^{\rho}$. The values were computed using equation (3.32) using the computed value of $M(\mu, \rho)$ from table 3.1.

Because of equations (3.27) , (3.28a), and (3.28b) it is hoped that for sufficiently large N, $\Theta(\delta, \mu, N, \rho)$ can be found. Since $M(\mu, \rho)$ can be estimated and $\mathcal{B}(x, 1-\rho)$, $\mathcal{B}(x, 2-\rho)$, and $\mathcal{B}(x, 3-\rho)$ are known functions, $\Theta(\delta, \mu, N, \rho)$ is easily determined. Table 3.2 shows specific values of Θ for different values of ρ, δ, and N. Figures 3.2, 3.3,and 3.4 plot Θ versus different arguments. Each plot in figure 3.2 shows that the value of Θ decays exponentially with an increase in δ for different values of ρ. Figure 3.3 compares the rates of decay of Θ with respect to δ for $\rho = 3, 4, 5$. Figure 3.4 shows that Θ also decays exponentially with respect to N. The rate of decay of Θ with respect to N does not vary for different values of ρ.

3.4. Dominant Features. Definition 3.2. *Given a region Ω, a function $g(x)$ is call the* **dominant feature** *of the function $f(x)$ in the region Ω, if*

$$\forall x \in \Omega, \left| \frac{f(x) - g(x)}{\max_{x\in\Omega} |g(x)|} \right| \ll 1. \tag{3.33}$$

Lemma 3.3. *Given a positive band pass filter of order $\rho \geq 3$ and given a function $f(x)$, which is of the form*

$$f(x) = \sum_{j=0}^{P} \left(A_j a(x - \xi_j) + B_j b(x - \xi_j) + C_j c(x - \xi_j)\right) + S(x). \tag{3.34}$$

If the minimum distance between any two shocks is greater than $\Theta(\delta, \mu, N, \rho)$ [equation (3.32)], then $A_j\, a_N^{\mu}(x - \xi_j)$ is the dominant feature of the function $f_N^{\mu}(x)$ in the region $\Omega_j = [\xi_j - 2\pi/N, \xi_j + 2\pi/N]$

Proof. Equation (3.34) is just a restatement of Lemma 1.1. Without loss of generality, search for the *dominate feature* in Ω_0.

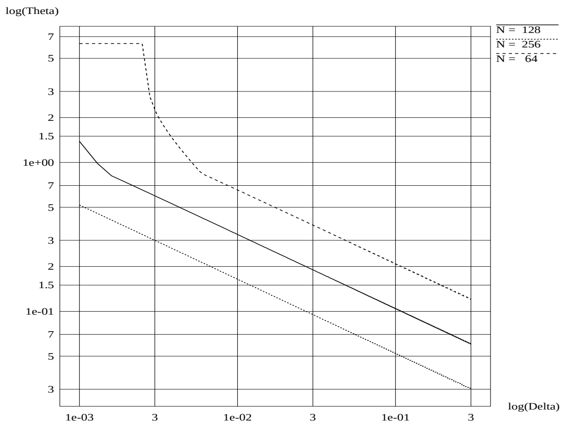

Figure (A)↗

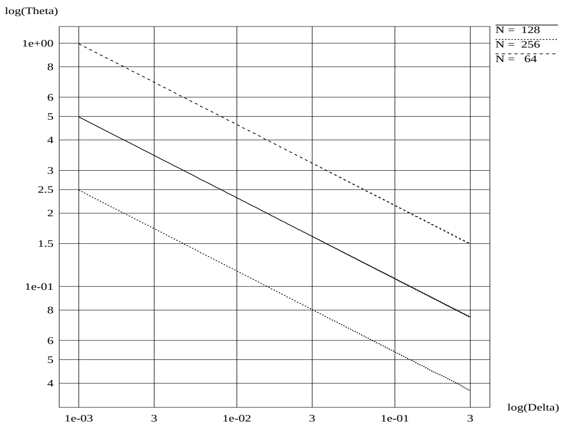

Figure (B)↗

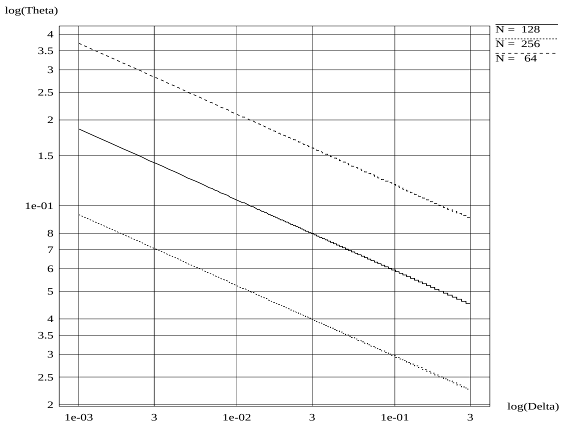

Figure (C)↗

Fig. 3.2: Plots of $\Theta(\delta, \mu, N, \rho)$ for varying values of δ. Figure (A) has $\rho = 3$, figure (B) has $\rho = 4$ and figure (C) has $\rho = 5$. Each figure shows the value of $\Theta(\delta, \mu, N, \rho)$ for three values of N for $\delta \in [.01, .2]$

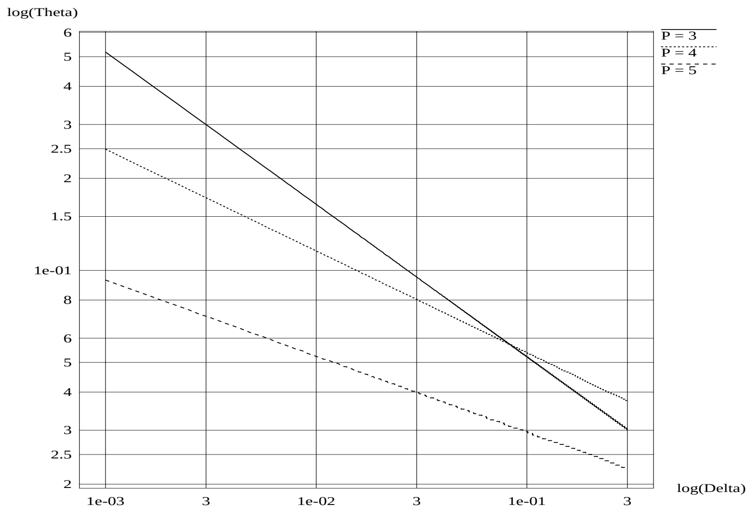

Fig. 3.3: Computed values of $\Theta(\delta, \mu, N, \rho)$ for $\delta \in [.01, .2]$ and three different values of ρ (3,4,5).

First consider the case with only one shock, $j = 0$. From (3.24),

$$f_N^\mu(x) = A_0 a_N^\mu(x - \xi_0) + \mathcal{O}\left(N^{-1}\right). \tag{3.35}$$

Recall the fact that $\mu(\omega)$ was normalized by $a_N^\mu(\pi/N)$. Therefore

$$\max_{x \in [-\pi/N, \pi/N]} |a_N^\mu(x)| \geq 1. \tag{3.36}$$

This results in

$$\left| \frac{f_N^\mu(x) - A_0\, a_N^\mu(x - \xi_0)}{A_0 \max_{x \in \Omega_0} |a_N^\mu(x)|} \right| = \left| \frac{\mathcal{O}\left(N^{-1}\right)}{A_0 \max_{x \in \Omega_0} |a_N^\mu(x)|} \right| \tag{3.37a}$$

$$\leq \left| \mathcal{O}\left(N^{-1}\right) \right| / |A_0|. \tag{3.37b}$$

Because of the assumptions on $f(x)$, $|A_0| = \mathcal{O}(1)$, and therefore $A_0\, a_N^\mu(x - \xi_0)$ is the dominant feature for $x \in \Omega_0$.

Now consider multiple shocks. If the shocks are further away than $\Theta(\delta, \mu, N, \rho)$, the contribution from other shocks will be much less than $a_N^\mu(x)$ for $x \in \Omega_0$. Therefore $A_0\, a_N^\mu(x - \xi_0)$ is still the dominant feature of $f_N^\mu(x)$ for $x \in \Omega_0$. $\square$

Definition 3.3. *Given a function $f(x)$ with $P + 1$ discontinuities at the locations ξ_j, define*

$$d(x; f) = \inf\{|x - (\xi_m + 2k\pi)|; 0 \leq m \leq P, k \in \mathcal{R}\}. \tag{3.38}$$

$d(x; f)$ is the distance from any shock. If there is only one shock at $x = 0$, then

$$d(x; f) = \begin{cases} x & \text{for } 0 \leq x \leq \pi \\ 2\pi - x & \text{for } \pi \leq x \leq 2\pi. \end{cases} \tag{3.39}$$

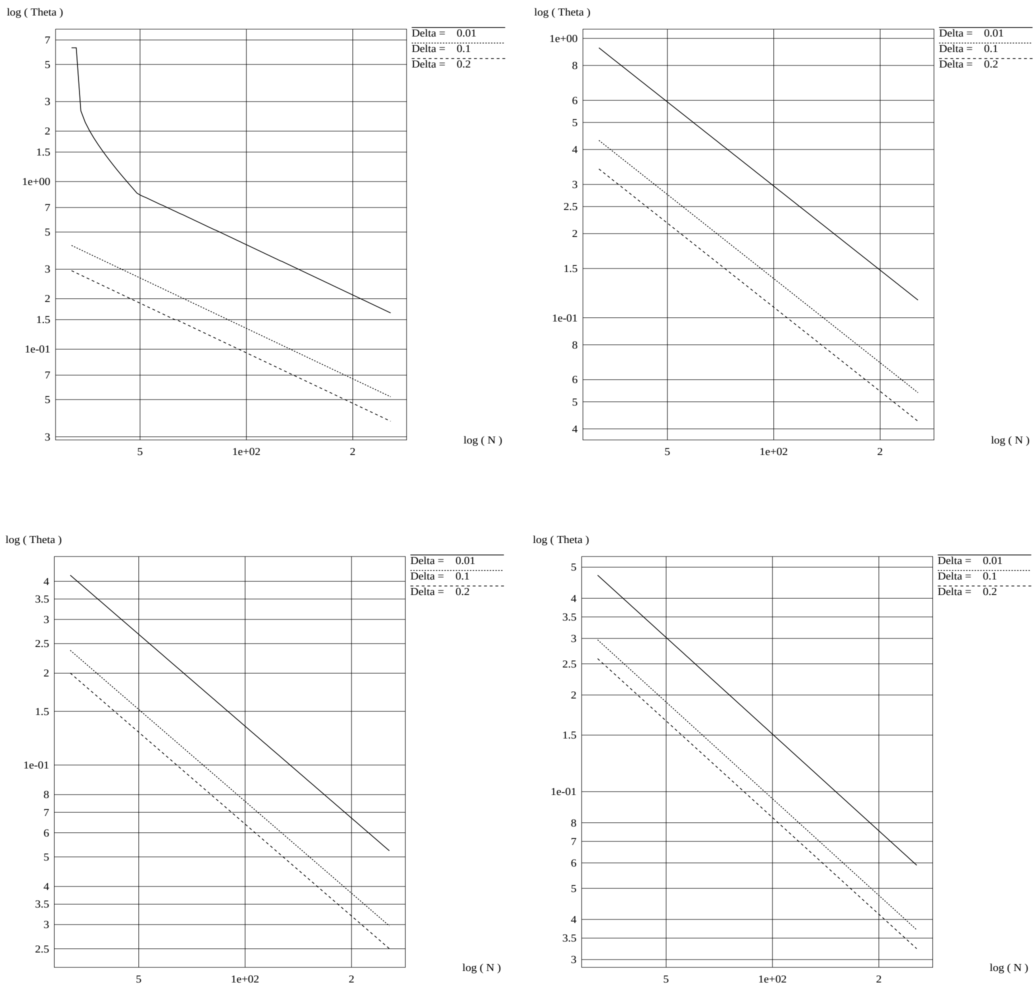

(A)↗ ↖(B)

(C)↗ ↖(D)

Fig. 3.4: Values of $\Theta(\delta, \mu, N, \rho)$ for varying values of N. The values of ρ are 3,4,5 and 6 are in figures (A), (B), (C), and (D), respectively. Values of N are $[32, 256]$. Each plot has three different values of δ, $(.01, .1, .2)$.

Lemma 3.4. *Given a non–negative band pass filter of order $\rho \geq 3$ and a function $f(x)$. Define $\mathcal{X}$ as the set of all points x which are at least $\Theta(\delta, \mu, N, \rho)$ distance from any shock. ie.*

$$\mathcal{X} = \{x; d(x, f) \geq \Theta(\delta, \mu, N, \rho)\} \tag{3.40}$$

Then

$$\forall x \in \mathcal{X}, |f_N^{\mu}(x)| \ll 1. \tag{3.41}$$

Proof. This is a direct result of the definition of $\Theta(\delta,\mu,N,\rho)$ and equation (3.12).

$$f_N^\mu(x) = \sum_{p=0}^{P} [A_p\, a_N^\mu(x-\xi_j) + B_p\, b_N^\mu(x-\xi_j) + C_p\, c_N^\mu(x-\xi_j)] + S_N^\mu(x) \tag{3.42}$$

$$|f_N^\mu(x)| \le \sum_{p=0}^{P} \delta(|A_p| + |B_p| + |C_p|) + \mathcal{O}\left(N^{1-\min(\rho,4)}\right) \tag{3.43}$$

Recall that $\delta \ll 1$, then

$$|f_N^\mu(x)| \ll 1. \tag{3.44}$$

□

Now it is possible to know what $f_N^\mu(x)$ looks like throughout the domain.

$$f_N^\mu(x) \approx \begin{cases} A_j\, a_N^\mu(x-\xi_j) & \text{if } x \in \Omega_j \\ 0 & \text{for } x \notin \mathcal{X} \end{cases} \tag{3.45}$$

4. Cell Shock Location. Given a 2π periodic function $f(x)$, project $f(x)$ onto $\mathcal{B}_N$ and then compute the Fourier Coefficients $\hat{f}(k)$ for $k \in [-N,N]$. Let $\mu^1(\omega)$, $\mu^2(\omega)$, $\mu^3(\omega)\ldots\mu^q(\omega)$ be the sequence of non–negative band pass filters of degree at least three. Choose a number of samples to take of the function $f_N^\mu(x)$, $M \ge N$. Define the discrete sequence

$$f_N^{\mu^q}(y_k) = \sum_{k=-N}^{N} \mu_k^q \hat{f} \tag{4.1a}$$

$$y_k = \frac{2\pi k}{M.} \tag{4.1b}$$

This can be computed quickly by using an FFT of length M.

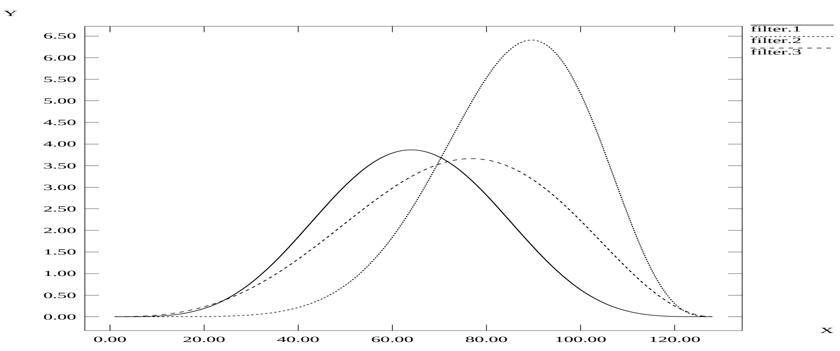

Fig. 4.1: Examples of filters μ^1, μ^2 and μ^3 used for the Cell Shock Location.

In order to find similarities between these functions $f_N^{\mu^1}(y_k)\ldots f_N^{\mu^q}(y_k)$, take the *min_mod*

$$\mathit{min\_mod}(x_1,x_2,x_3..x_n) = \begin{cases} \min(x_1,x_2,x_3..x_n) & \text{if } \forall i,\ x_i > 0 \\ \max(x_1,x_2,x_3..x_n) & \text{if } \forall i,\ x_i < 0 \\ 0 & \text{otherwise} \end{cases} \tag{4.2}$$

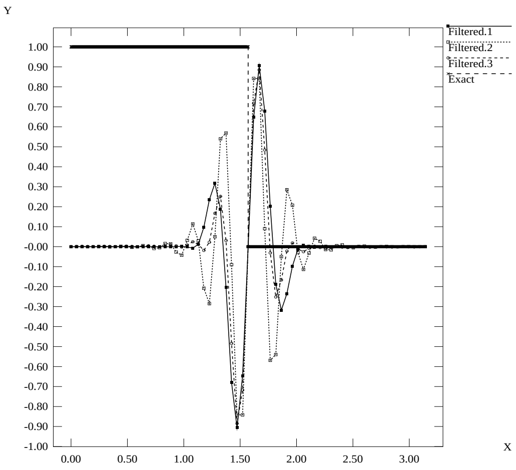

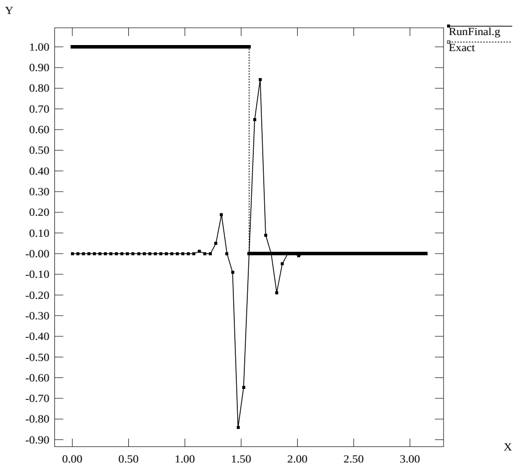

Fig. 4.2: [left] $f_N^{\mu^1}(y_k)$, $f_N^{\mu^2}(y_k)$ and $f_N^{\mu^3}(y_k)$, where $f(x)$ is a step function.

Fig. 4.3: [right] $F(y_k) = min\_mod\left\{f_N^{\mu^1}(y_k), f_N^{\mu^2}(y_k), f_N^{\mu^3}(y_k)\right\}$.

of their discrete values. Define,

$$F(y_k) = min\_mod(f_N^{\mu^1}(y_k), f_N^{\mu^2}(y_k) \dots f_N^{\mu^q}(y_k)). \tag{4.3}$$

LEMMA 4.1. *Given a function $f(x)$, a set of non-negative band pass filters $\mu^1(\omega) \dots \mu^q(\omega)$ and $F(y_k)$ as defined in equation (4.3). Then for points y_k, such that $d(y_k; f) \approx \pi/N$, $|F(y_k)| = \mathcal{O}(1)$, and for points y_k, such that $d(y_k; f) \geq \Theta(\mu, N, \rho)$, $|F(y_k)| \ll 1$. Furthermore, if y_l is such that $d(y_l; f) \approx \pi/N$ and to the left of the closest shock, and y_r is such that $d(y_r; f) \approx \pi/N$ and is to the right of the same shock, then $F(y_l)\,F(y_r) < 0$. (ie. $F(y_l)$ and $F(y_r)$ have opposite signs.)*

Proof. To show that $|f_N^{\mu}(y_k)| = \mathcal{O}(1)$ for $d(y_k; f) \approx \pi/N$:
This is a result of Lemma 3.3 and the properties of $a_N^{\mu}(x)$. Without loss of generality, let ξ_0 be the shock closest to y_k, then since $d(y_k; f) \leq 2\pi/N$,

$$f_N^{\mu}(y_k) \approx A_0\, a_N^{\mu}(y_k) + \mathcal{O}\left(N^{-1}\right). \tag{4.4}$$

Since $|a_N^{\mu}(\pi/N)|$ is close to the maximum of $|a_N^{\mu}(x)|$ and y_k is close to π/N, then $|a_N^{\mu}(y_k)|$ is close to the maximum of $|a_N^{\mu}(x)|$. Therefore $|a_N^{\mu}(y_k)| \approx 1$, and

$$|f_N^{\mu}(y_k)| \approx |A_0|. \tag{4.5}$$

$|f(y_k)| \ll 1$ is a result of Lemma 3.4.

$F(y_l)\,F(y_r) < 0$, where y_l is slightly left of the shock and y_r is slightly right of the shock is a result of using even band pass filters and is easy to see from the examples so far. $\square$

This lemma describes how $F(y_k)$ will behave for a collection of band pass filters. However, for a clear view of shock location like in figure 4.3, μ^k should be chosen similar to the filters listed in table 1.4.1 and shown in figure 4.1.

4.1. Actual Computation of Cell Shock Location.

Cell Shock Location Procedure

Input:

1. $\hat{f}(k)$, for $k = -N, \ldots, N$, $2N+1$ Fourier coefficients
2. $\mu^q(k/N)$, q different band pass filters
3. $\mathcal{K}$, parameter chosen to eliminate small scale features (≈ 3)
4. M, the number of points to evaluate $f_N^{\mu^q}(x)$ at ($\approx 4N$)

Compute:

1. $F_j^q = f_N^{\mu^q}\left(\frac{2\pi j}{M}\right)$, for $j = 0, \ldots, M-1$
2. $F(j) = min\_mod_q\left(F_j^q\right)$
3. $\overline{F} = \sum_j |F(j)|$
4. $\overline{\Theta} = \min_q\left(\Theta(\mu^q, N, \rho_q)\right)$

Find the set $\Lambda\{j\}$ such that if $j \in \Lambda$, then either

1. $F(j) > \mathcal{K}\,\overline{F}$ and
2. $F(j+k) < -\mathcal{K}\,\overline{F}$ for $k = 1, 2, \text{or } 3$

or

1. $F(j) < -\mathcal{K}\,\overline{F}$ and
2. $F(j+k) > \mathcal{K}\,\overline{F}$ for $k = 1, 2, \text{or } 3$

Eliminate j or k from Λ if $|j-k| > \overline{\Theta}\,M/2\pi$.

The size of Λ is the number of shocks in the data and a very rough estimate of the location of the j^{th} shock is $\pi(2j+1)/M$. The Cell Shock Location estimate of the location of the j^{th} shock is now obtained by finding the zero of $f_N^{\mu^0}(x)$ closest to $\pi(2j+1)/M$. The final requirement on elements of Λ ensures that the method doesn't find the same shock twice (μ^0 denotes that one of the initial band pass filters is used to find the Cell Shock Location estimate.)

5. Analysis of Multiple Shocks and Sub–Cell Filters. The previous procedure produces initial estimates for shock locations. The filters used before where non-negative. This requirement is necessary to ensure that the function has the dominant minima and maxima around the shock. However this limits the accuracy of the method. Recall that in the second example that $f_N^{\mu}(0) = B\sum_k \mu(k/N)\,\beta_k$. Since β_k is strictly positive and $\mu(k/N)$ was also positive, then $f_N^{\mu}(0) \neq 0$. However in this section a new filter will be found such that $f_N^{\nu}(\xi_k) \approx 0$.

Given a function $f(x)$ with shock locations ξ_i for $i = 0 \ldots P$, to examine the effect of filtering

$f(x)$. Write $f(x)$ as

$$f(x)=\sum_{k=0}^{P}\left(A_k\, a(x-\xi_k)+B_k\, b(x-\xi_k)+C_k\, c(x-\xi_k)\right)+S(x) \tag{5.1}$$

where $S(x)\in\mathcal{C}^3$. Project $f(x)$ onto $\mathcal{P}_N$ and then filter

$$f_N^\nu(x)=\sum_{k=0}^{P}\left(A_k\, a_N^\nu(x-\xi_k,\nu,N)+B_k\, b_N^\nu(x-\xi_k)+C_k\, c_N^\nu(x-\xi_k)\right)+S_N^\nu(x). \tag{5.2}$$

The goal is to find a filter for which $f_N^\nu(\xi_k)\approx 0$. Without loss of generality, evaluate $f_N^\nu(x)$ at $x=\xi_0$.

$$f_N^\nu(\xi_0)=\sum_{k=0}^{P}\left(A_k\, a_N^\nu(\xi_0-\xi_k)+B_k\, b_N^\nu(\xi_0-\xi_k)+C_k\, c_N^\nu(\xi_0-\xi_k)\right)+S_N^\nu(\xi_0). \tag{5.3}$$

The goal is to minimize $|f_N^\nu(\xi_0)|$. The equation

$$|f_N^\nu(\xi_0)|\le\sum_{k=0}^{P}\left\{|A_k|\,|a_N^\nu(\xi_0-\xi_k)|+|B_k|\,|b_N^\nu(\xi_0-\xi_k)|+|C_k|\,|c_N^\nu(\xi_0-\xi_k)|\right\}+|S_N^\nu(\xi_0)| \tag{5.4}$$

is easier to minimize than equation (5.3). To minimize equation (5.4), one needs only to minimize each of these different quantities, $a_N^\nu(0)$, $b_N^\nu(0)$, $c_N^\nu(0)$, $a_N^\nu(\xi_0-\xi_k)$, $b_N^\nu(\xi_0-\xi_k)$, $c_N^\nu(\xi_0-\xi_k)$, and $S_N^\nu(x)$. At the this point consider the filter ν to be a discrete filter and write each of these quantities in terms of ν_k.

5.1. Analysis of $\mathbf{a_N^\nu(0)}$, $\mathbf{b_N^\nu(0)}$, and $\mathbf{c_N^\nu(0)}$. This section is quite easy. Since ν_k is an even filter, $a_N^\nu(0)=0$ and $c_N^\nu(0)=0$, and the only term left is $b_N^\nu(0)$,

$$|b_N^\nu(0)|=\left|\sum_{k=1}^{N}\frac{\nu_k}{k^2}\right|. \tag{5.5}$$

The minimization problem considered here minimizes the sum of the squares of each term. Therefore write the bound on $b_N^\nu(0)$ as

$$|b_N^\nu(0)|^2=\left(\sum_{k=1}^{N}\frac{\nu_k}{k^2}\right)^2=\sum_{j=1}^{N}\sum_{k=1}^{N}\frac{\nu_k\nu_j}{(jk)^2}. \tag{5.6}$$

5.2. Analysis of $\mathbf{a_N^\nu(\xi_0-\xi_k)}$, $\mathbf{b_N^\nu(\xi_0-\xi_k)}$, and $\mathbf{c_N^\nu(\xi_0-\xi_k)}$. Now assume there exists a minimal distance between any two shocks, Θ. Then

$$\begin{aligned}|a_N^\nu(\xi_0-\xi_k)|&\le\max_{x\in[\Theta,\pi]}|a_N^\nu(x)|\\ |b_N^\nu(\xi_0-\xi_k)|&\le\max_{x\in[\Theta,\pi]}|b_N^\nu(x)|\\ |c_N^\nu(\xi_0-\xi_k)|&\le\max_{x\in[\Theta,\pi]}|c_N^\nu(x)|.\end{aligned} \tag{5.7}$$

The goal is to find a minimization of the right hand side in terms of ν_k. Since the right hand side is a maximum over most of the domain, the resulting filter will be a Global Sub-Cell filter.

Using the fact

$$\left(\max_{x\in[a,b]}|f(x)|\right)^2 \le 2|f(a)|^2 + 2(b-a)\int_a^b \left(f'(x)\right)^2 dx \tag{5.8}$$

results in the following bounds,

$$\begin{aligned}
\frac{1}{2}|a_N^\nu(\xi_0-\xi_k)|^2 &\le \left(a_N^\nu(\Theta)\right)^2 + (\pi-\Theta)\int_\Theta^\pi \left(\frac{\partial}{\partial x}a_N^\nu(x)\right)^2 dx\\
\frac{1}{2}|b_N^\nu(\xi_0-\xi_k)|^2 &\le \left(b_N^\nu(\Theta)\right)^2 + (\pi-\Theta)\int_\Theta^\pi \left(\frac{\partial}{\partial x}b_N^\nu(x)\right)^2 dx\\
\frac{1}{2}|c_N^\nu(\xi_0-\xi_k)|^2 &\le \left(c_N^\nu(\Theta)\right)^2 + (\pi-\Theta)\int_\Theta^\pi \left(\frac{\partial}{\partial x}c_N^\nu(x)\right)^2 dx.
\end{aligned} \tag{5.9}$$

The bounds above can be re-written in terms of ν_k using these relationships,

$$\begin{aligned}
\int_\Theta^\pi \left(\frac{\partial}{\partial x}a_N^\nu(x)\right)^2 &= \sum_{j=1}^N\sum_{k=1}^N \nu_j\nu_k \int_\Theta^\pi \cos(kx)\cos(jx)dx\\
\int_\Theta^\pi \left(\frac{\partial}{\partial x}b_N^\nu(x)\right)^2 &= \sum_{j=1}^N\sum_{k=1}^N \frac{\nu_j\nu_k}{jk} \int_\Theta^\pi \sin(kx)\sin(jx)dx\\
\int_\Theta^\pi \left(\frac{\partial}{\partial x}c_N^\nu(x)\right)^2 &= \sum_{j=1}^N\sum_{k=1}^N \frac{\nu_j\nu_k}{(jk)^2} \int_\Theta^\pi \cos(kx)\cos(jx)dx
\end{aligned} \tag{5.10}$$

$$\begin{aligned}
\left(a_N^\nu(\Theta)\right)^2 &= \sum_{j=1}^N\sum_{k=1}^N \nu_j\nu_k \left(\frac{\sin(j\Theta)}{j}\frac{\sin(k\Theta)}{k}\right)\\
\left(b_N^\nu(\Theta)\right)^2 &= \sum_{j=1}^N\sum_{k=1}^N \nu_j\nu_k \left(\frac{\cos(j\Theta)}{j^2}\frac{\cos(k\Theta)}{k^2}\right)\\
\left(c_N^\nu(\Theta)\right)^2 &= \sum_{j=1}^N\sum_{k=1}^N \nu_j\nu_k \left(\frac{\sin(j\Theta)}{j^3}\frac{\sin(k\Theta)}{k^3}\right).
\end{aligned} \tag{5.11}$$

Define

$$\Lambda_{j,k}(\Theta,\pi) = 2\,(\pi-\Theta)\int_\Theta^\pi \cos(kx)\cos(jx)dx + 2\,\frac{\sin(j\Theta)}{j}\frac{\sin(k\Theta)}{k} \tag{5.12a}$$

$$\Gamma_{j,k}(\Theta,\pi) = 2\,(\pi-\Theta)\int_\Theta^\pi \sin(kx)\sin(jx)dx + 2\,\frac{\cos(j\Theta)}{j}\frac{\cos(k\Theta)}{k}. \tag{5.12b}$$

The bounds then become

$$\begin{aligned}
|a_N^\nu(\xi_0-\xi_k)|^2 &\le \sum_{j=1}^N\sum_{k=1}^N \nu_j\Lambda_{j,k}\nu_k\\
|b_N^\nu(\xi_0-\xi_k)|^2 &\le \sum_{j=1}^N\sum_{k=1}^N \frac{\nu_j}{j}\Gamma_{j,k}\frac{\nu_k}{k}\\
|c_N^\nu(\xi_0-\xi_k)|^2 &\le \sum_{j=1}^N\sum_{k=1}^N \frac{\nu_j}{j^2}\Lambda_{j,k}\frac{\nu_k}{k^2}.
\end{aligned} \tag{5.13}$$

LEMMA 5.1. **$\mathbf{\Lambda}$** *and* **$\mathbf{\Gamma}$** *are symmetric positive semi–definite matrixes.*

Proof. The proof is elementary given the definitions of these matrices. ∎

5.3. Analysis of $\mathbf{S}_{\mathbf{N}}^{\nu}(\mathbf{x})$.

$$S_N^{\nu}(x) = \sum_{k=-N}^{N} \nu_k \hat{S}_k e^{\imath kx}. \tag{5.14}$$

Using the fact that $|\hat{S}_k| < \mathcal{K}/k^4$, for some $\mathcal{K}$, find a bound on $|S_N^{\nu}(x)|^2$.

$$|S_N^{\nu}(x)|^2 = \left| \sum_{k=-N}^{N} \hat{S}_k \; \nu_k \; e^{\imath kx} \right|^2 \tag{5.15a}$$

$$= \left| \sum_{k=-N}^{N} k^4 \hat{S}_k \; \frac{\nu_k}{k^4} \; e^{\imath kx} \right|^2 \tag{5.15b}$$

$$\leq \left(\sum_{k=-N}^{N} \left| k^4 \hat{S}_k \right|^2 \right) \left(\sum_{k=-N}^{N} \left| \frac{\nu_k}{k^4} \right|^2 \right) \tag{5.15c}$$

$$\leq \left(\sum_{k=-N}^{N} \mathcal{K}^2 \right) \left(\sum_{k=-N}^{N} \left| \frac{\nu_k}{k^4} \right|^2 \right) \tag{5.15d}$$

$$\leq \mathcal{K}^2 \left(\sum_{k=-N}^{N} 1 \right) \left(\sum_{k=-N}^{N} \frac{\nu_k^2}{k^8} \right) \tag{5.15e}$$

$$|S_N^{\nu}(x)|^2 \leq 2\mathcal{K}^2(2N+1) \left(\sum_{k=1}^{N} \frac{\nu_k^2}{k^8} \right) \tag{5.16}$$

Equation (5.16) is obviously a symmetric positive definite matrix since it is a diagonal matrix with only positive entries.

5.4. Total Error. The goal was to minimize (5.4). But the equation

$$|f_N^{\nu}(\xi_q)|^2 \leq \mathcal{M}^2 \left\{ |b_N^{\nu}(0)|^2 + \max_x \left[|S_N^{\nu}(x)|^2 \right] + \max_{x \in [\Theta, \pi]} \left[|a_N^{\nu}(x)|^2 + |b_N^{\nu}(x)|^2 + |c_N^{\nu}(x)|^2 \right] \right\} \tag{5.17}$$

$$\mathcal{M} = (P+1) \cdot \max_{k=0\dots P} \left\{ 1, |A_k|, |B_k|, |C_k|, \frac{2\mathcal{K}}{\sqrt{P+1}} \right\}. \tag{5.18}$$

is as effective and easier to bound than (5.4). Substitute equations (5.6), (5.14) & (5.16) into equation (5.17). This results in one equation to be minimized with respect to ν_k,

$$|f_N^{\nu}(\xi_q)|^2 \leq \mathcal{M}^2 \left\{ \sum_{j=1}^{N} \sum_{k=1}^{N} \nu_j \nu_k \left[\frac{1}{(jk)^2} + \left(\Lambda_{j,k} + \frac{\Gamma_{j,k}}{jk} + \frac{\Lambda_{j,k}}{(jk)^2} \right) + (2N+1) \frac{\nu_j^2}{j^8} \right] \right\}. \tag{5.19}$$

This can be re-written as

$$|f_N^{\nu}(\xi_q)|^2 \leq \mathcal{M}^2 \sum_{j=1}^{N} \sum_{k=1}^{N} \nu_j \Xi_{j,k} \nu_k \tag{5.20a}$$

$$\Xi_{j,k} = \frac{1}{(jk)^2} + \left(\Lambda_{j,k} + \frac{\Gamma_{j,k}}{jk} + \frac{\Lambda_{j,k}}{(jk)^2} \right) + \delta_{j,k} \, \frac{2N+1}{j^8} \tag{5.20b}$$

Because $\mathbf{\Xi}$ is the sum of 4 symmetric positive semi–definite matrices and a symmetric positive definite matrix, $\mathbf{\Xi}$ is also a symmetric positive definite matrix. To find ν_k which minimizes equation (5.20b), one needs only find the eigenvectors of $\mathbf{\Xi}$. (See [1] and [16])

5.5. Bounds on $|\mathbf{f}^{\nu}_{\mathbf{N}}(\xi_{\mathbf{q}})|^2$. While very good computational bounds have been found, analytical bounds on $|f^{\nu}_N(\xi_q)|^2$ as a function of Θ and N have not been found. Figure 5.1 shows that the computed maximum of $|f^{\nu}_N(\xi_q)|^2$ as both functions of Θ and N. The maximum of $|f^{\nu}_N(\xi_q)|^2$ decreases as Θ or N increases.

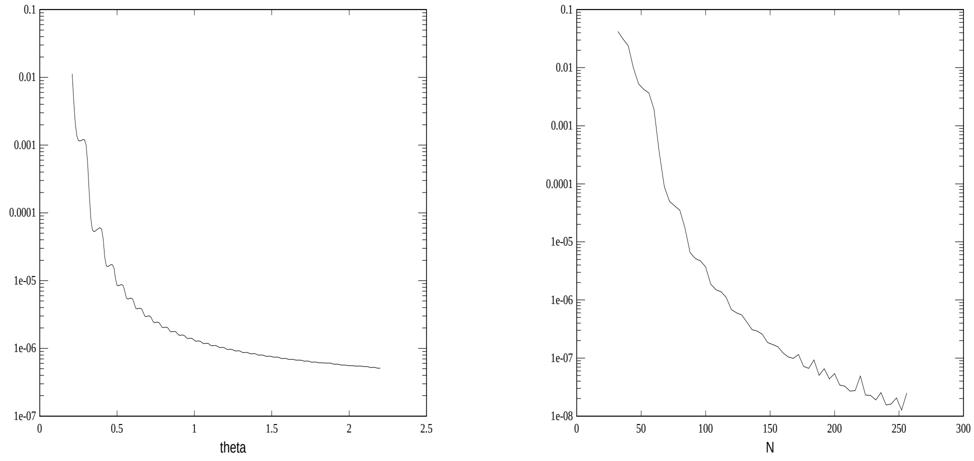

Fig. 5.1: [Left] Plot of the maximum value of $|f^{\nu}_{64}(\xi_q)|^2$ as a function of Θ. [Right] Plot of the maximum value of $|f^{\nu}_N(\xi_q)|^2$ as a function of N for $\Theta = .3$. [f(x) = a(x) + b(x) + c(x) or equation (5.20b) with $\mathcal{M} = 1$.]

The Global filter was used to compute the maximum error in finding two shocks. The first shock is located at $x = 1$, the second shock's location varies from $x = 1.3$ to $x = 4.1$. Doubling the number of points leads to the error being reduced by more that an order of magnitude. This seems to indicate that the method is at least 3^{rd} order. This is surprising since the filter was designed to account for the discontinuities in the function and it's first and second derivatives. That should lead to a method which is 3^{rd} order. But the actual computations have shown slightly higher accuracy. I think that once an analytical representation of $|f^{\nu}_N(\xi_q)|^2$ in terms of Θ and N is found, this will be explained.

5.6. Local Filter. In a previous section the assumption that there was a Θ such that $|\xi_j - \xi_k| \geq \Theta$ $(j \neq k)$ was essential to the definition of a Global Sub–Cell Filter. Typically $\Theta = .3$ which gives a minimization problem which finds a 2π–periodic function which is close to zero for 90% of the domain.

A Global Filter places a heavy restrictions on the minimal value for $|f^{\nu}_N(\xi_0)|^2$. A way to lessen the restriction is to change the domain by which $a^{\nu}_N(x)$, $b^{\nu}_N(x)$, and $c^{\nu}_N(x)$ are bounded. Instead of bounding them for all $x \in [\Theta, \pi]$, bound them in neighborhoods about $\xi_j - \xi_k$.

It is obvious that ξ_k is not known, but first estimates from the Cell Shock Location will provide

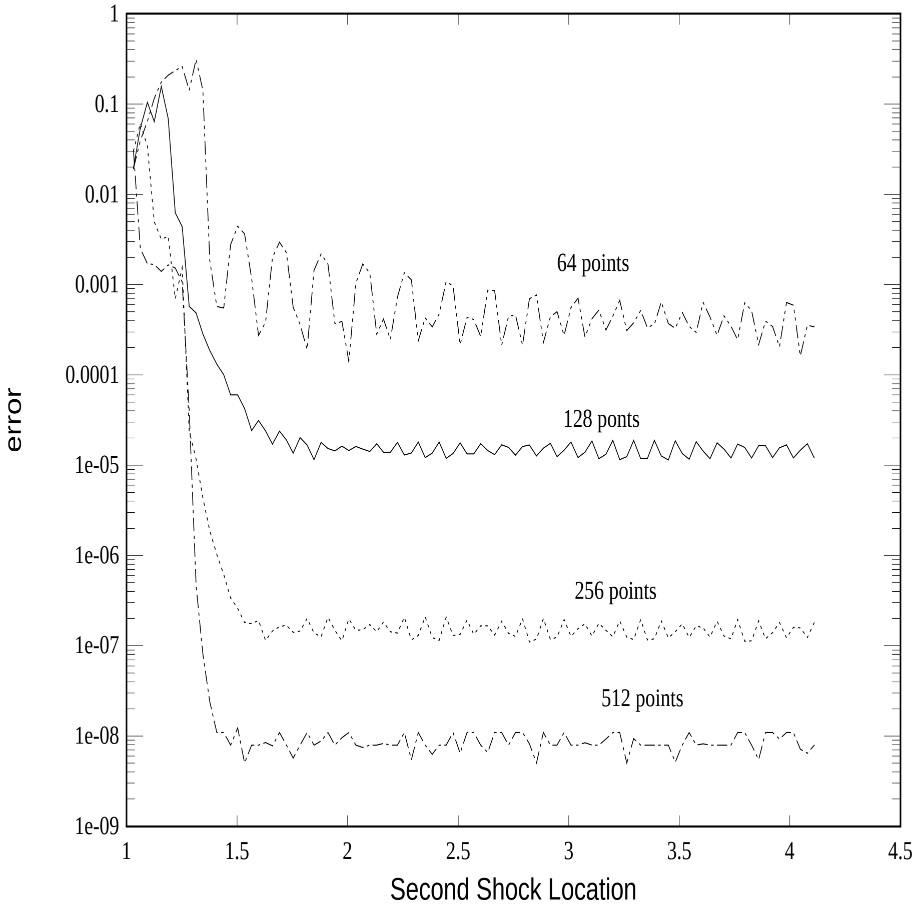

Fig. 5.2: Maximum error in finding two different shocks. The error is plotted on the y–axis while the location of the second shock is plotted on the x–axis. Since $\Theta = .3$, accurate results for this problem for the second shock located between $x = 1$ and $x = 1.3$ are not expected. Outside this range, the error decreases quickly as the number of points is increase.

enough information to define the proper range for Ω. Define $\Omega(\delta)$ as

$$\Omega(\delta) = \bigcup_{k=0}^{P} \bigcup_{j=k+1}^{P} [\xi_j - \xi_k - \delta, \xi_j - \xi_k + \delta]. \tag{5.21}$$

Also define $\eta_{j,k} = \xi_j - \xi_k - \delta$ ($\delta \approx \frac{2\pi}{2N+1}$). Then redefine $\Lambda_{j,k}$ and $\Gamma_{j,k}$ as

$$\Lambda_{j,k}(\Omega) = 2\sum_{q=0}^{P} \sum_{p=q+1}^{P} \left(\frac{\sin(j\eta_{q,p})}{j} \frac{\sin(k\eta_{q,p})}{k} \right) + 2|\Omega(\delta)| \int_{\Omega(\delta)} \cos(kx)\cos(jx)dx$$

$$\Gamma_{j,k}(\Omega) = 2\sum_{q=0}^{P} \sum_{p=q+1}^{P} \left(\frac{\cos(j\eta_{q,p})}{j} \frac{\cos(k\eta_{q,p})}{k} \right) + 2|\Omega(\delta)| \int_{\Omega(\delta)} \sin(kx)\sin(jx)dx.$$

These can be used in (5.19) and (5.20b) resulting in a new $\Xi(\Omega)$. A formal proof showing that $\Xi(\Omega)$ is symmetric positive definite can be shown the same way as in the Global Sub–Cell Filter. A filter which restricts the set Ω on which $a_N^\nu(x)$, $b_N^\nu(x)$ and $c_N^\nu(x)$ are minimized will be call a Local Sub–Cell Filter.

EXAMPLES 5.1.
To demonstrate the increased accuracy, both the local and Global Sub–Cell Filters have been applied to two test functions.

I. $f_5(x)$ has 5 discontinuities in the data and is a piecewise 2^{nd} order polynomial between the discontinuities. (See figure 5.3)

$$f_5(x) = \begin{cases} 2 + x - 4x^2 & \textit{if } 1.0 < x < 1.5 \\ -5 + x + x^2 & \textit{if } 1.5 < x < 2.5 \\ 2 - 3x + 2x^2 & \textit{if } 2.5 < x < 3.5 \\ 1 - 2x + x^2 & \textit{if } 3.5 < x < 5.0 \\ 40 + x - x^2 & \textit{if } 5.0 < x < 2\pi + 1.0 \end{cases} \tag{5.23}$$

II. $f_{83}(x)$ has only three shocks and is analytic between the shocks. Both of the functions are used as test equations in Eckhoff's paper [6].

$$f_{83}(x) = \begin{cases} 0 & \textit{if } x < 0 \\ e^x & \textit{if } 1 < x < 2 \\ \sin(x/2) & \textit{if } 2 < x < 5 \\ 0 & \textit{if } 5 < x \end{cases} \tag{5.24}$$

Notice that both methods have excellent convergence, but the local filter's answers are noticeablely smaller. Both methods converge because of the results of equation (5.17). But the better results for the Local Filter are because the minimal value found for equation (5.20b) now depends on a smaller range. See table (5.1) for results.

Comparison of Local & Global Filters				
	Function $f_5(x)$ [*eqn. 5.23*]		Function $f_{83}(x)$ [*eqn. 5.24*]	
Points	Local Filter	Global Filter	Local Filter	Global Filter
64	7.24×10^{-3}	5.34×10^{-3}	1.40×10^{-5}	1.50×10^{-3}
128	2.59×10^{-6}	2.68×10^{-4}	1.44×10^{-6}	8.77×10^{-5}
256	1.07×10^{-7}	9.42×10^{-6}	5.62×10^{-9}	2.26×10^{-6}
512	3.21×10^{-7}	1.14×10^{-6}	3.14×10^{-9}	2.71×10^{-7}

Table 5.1: Results of using a Global and Local Sub–Cell Filter to further refine shock estimates.

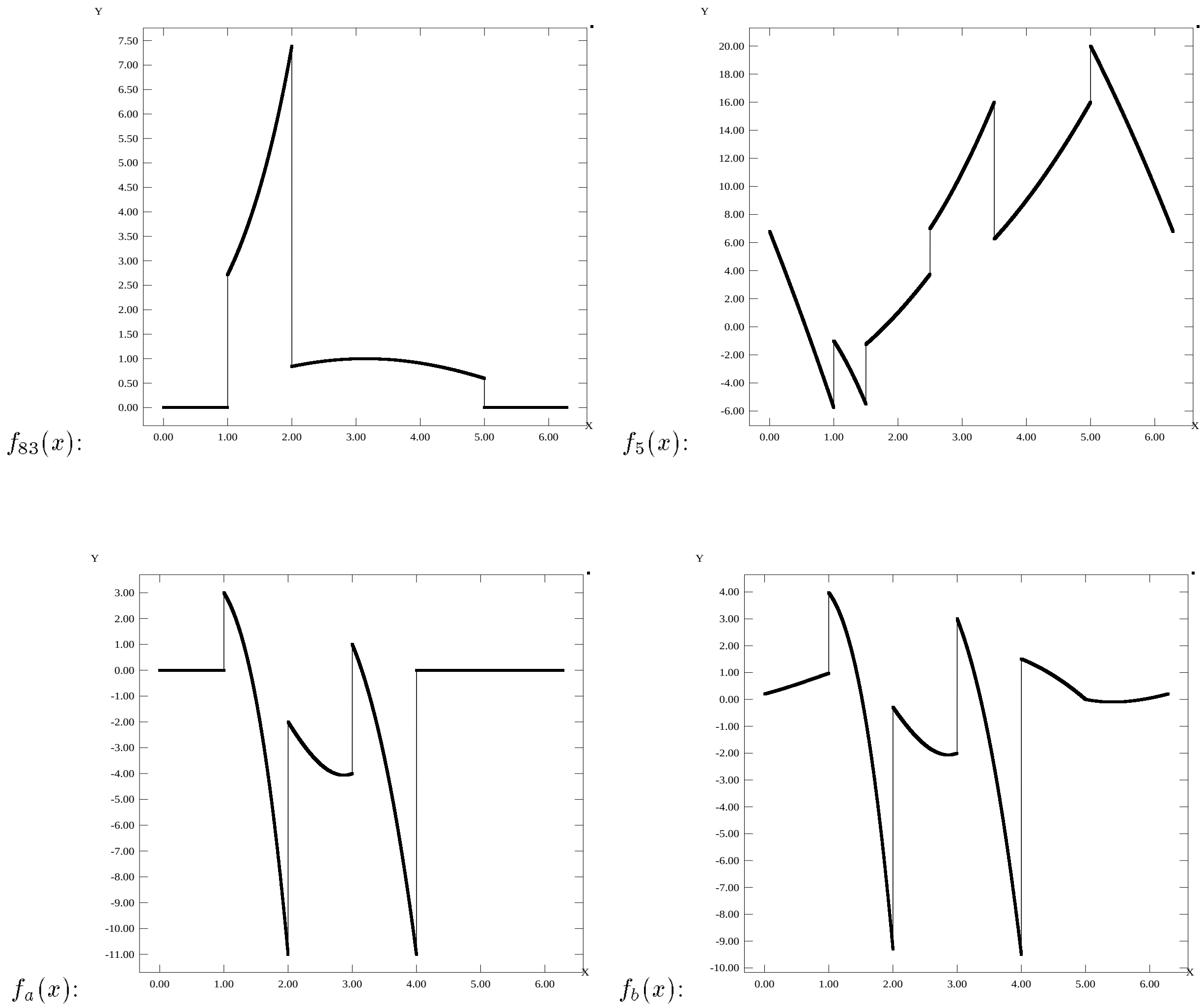

Fig. 5.3: These are four of the test functions which were used to test the Sub–Cell Filter Shock Location Technique. Clockwise from top left are $f_{83}(x)$, $f_5(x)$, $f_a(x)$, and $f_b(x)$.

5.7. Contact Discontinuities. The disadvantage of using a Local Sub–Cell Filter is that there is little control over the error if the data contains a contact discontinuity. As discussed in section 1.3, there are contact discontinuities of different strengths. The contact discontinuities considered here are continuous functions with discontinuous derivatives.

The Global Sub–Cell Filter assumes that every thing more than distance Θ away from a shock should be discounted. But the local Sub–Cell Filter only minimizes $a_N^\nu(x)$, $b_N^\nu(x)$ and $c_N^\nu(x)$ around the points $x = \xi_j - \xi_k$ $(j \neq k)$. However if a contact discontinuity exists, there is not enough information to know where to minimize $b_N^\nu(x)$ and $c_N^\nu(x)$ around.

Examples 5.2. *Shock Location involving a Contact Discontinuity*

I. *Theoretical.* *Let ξ_{-1} be the location of a contact discontinuity, and let ξ_0 and ξ_1 be the location of two other shocks. (Assume everything else is perfectly smooth.) Then the filtered function will be*

$$f_N^\nu(x) = A_0 a_N^\nu(x-\xi_0) + A_1 a_N^\nu(x-\xi_1) + B b_N^\nu(x-\xi_{-1}). \tag{5.25}$$

Since there the Cell Shock Location will only estimate ξ_0 and ξ_1, $\Omega = (|\xi_0-\xi_1|-\delta, |\xi_0-\xi_1|+\delta)$. Then evaluating at ξ_0

$$f_N^\nu(\xi_0) = A_0 a_N^\nu(0) + A_1 a_N^\nu(\xi_0-\xi_1) + B b_N^\nu(\xi_0-\xi_{-1}). \tag{5.26}$$

The first term is equal to zero. The Local Sub–Cell Filter ensures that the second term should be close to zero. But there is no knowledge of the magnitude of $b_N^\nu(\xi_0-\xi_{-1})$. Without an estimate of ξ_{-1}, a Local Sub–Cell Filter can't minimize it's effect.

II. *Computational.* *To demonstrate the problems of contact discontinuities consider applying both methods to two different functions. The first function, $f_a(x)$, has four shocks, and is piecewise 3rd order polynomials between the shocks.*

$$f_a(x) = \begin{cases} 0 & \text{if } 0.0 < x < 1.0 \\ 3+x+2x^2-3x^3 & \text{if } 1.0 < x < 2.0 \\ 2+4x-5x^2+x^3 & \text{if } 2.0 < x < 3.0 \\ 1-3x+4x^2-x^3 & \text{if } 3.0 < x < 4.0 \\ 0 & \text{if } 4.0 < x < 2\pi. \end{cases} \tag{5.27}$$

The second function, $f_b(x)$, is almost the same as $f_a(x)$ except that a contact discontinuity is added at $x=5$. (See figure 5.3)

$$f_b(x) = f_a(x) + 19\ b(x-5) - 16\ c(x-5) + 6\ d(x-5) \tag{5.28}$$

($d(x)$ is a smooth function with only a discontinuity in the 3^{rd} derivative.) Again both methods converge to the correct shock locations, but Table 5.2 shows that the local filter converges slower when there is a contact discontinuity.

5.8. Local vs. Global Sub–Cell Filter. There is a trade off. One can get a lower minimization using a Local Sub–Cell Filter, but accuracy goes down if there is a contact discontinuity. There is another difference between the Local and Global Filters. The Global Filter can be pre–computed or stored in memory. The Local Filter can not be computed until first estimates of the location of the shocks is known. If this filtering technique is to be run many times in the same program, pre–computing the filter would be quicker.

Comparison of Local & Global Filters (II)					
		$f_a(x)$ [*eqn. 5.27*]		$f_b(x)$ [*eqn. 5.28*]	
Points	Δx	Local Filter	Global Filter	Local Filter	Global Filter
64	.0982	7.12×10^{-3}	2.81×10^{-3}	1.94×10^{-2}	2.82×10^{-3}
128	.0491	8.40×10^{-7}	1.69×10^{-4}	2.08×10^{-3}	1.65×10^{-4}
256	.0245	3.01×10^{-8}	5.80×10^{-6}	1.66×10^{-3}	5.80×10^{-6}
512	.0123	1.01×10^{-9}	6.90×10^{-7}	6.67×10^{-4}	6.93×10^{-7}

Table 5.2: Results from using Global and Local Sub–Cell Filters to further refine shock location estimates when a contact discontinuity is present.

5.9. Number of non-zero elements of $\nu_\mathbf{k}$. An important improvement is setting some of the ν_k's equal to zero. (ie. $\nu_k = 0$ for $k \leq N/2$) This will reduce the computations which are needed to find the minimization. Local Sub–Cell Filters using only 10 non–zero ν_k's for each shock is sufficient to obtain very good results. All calculations are made using a Local Sub–Cell Filter use this ratio of 10 non–zero ν_k's to every shock.

6. Method applied to Physical Data . This section contains two different kinds of data and the Band Pass Shock Location Technique applied to each. The first set of data contains 1–D periodic atmospheric data. The data consists of un–filtered observational data, computational model data, and filtered observational data. The second data set is the result of a numerical procedure on a 2–D Chebyshev grid.

6.1. 1–D Periodic Data. These four sets of data consist of 96 data points and come from either observations or models of the Earth. The data is only one slice of the Earth (ie. one latitude). Data Set #1 is the observed wind speed, while Data Set #2 is the results of a computational model of the wind. Data Set #3 is the observed altitude and Data Set #4 is a low-pass filtered version of Data Set #3. Each of these data are plotted in figure 6.1 and the results are in table 6.1. Comparing the computed locations of the shocks to the plots, one notices that the estimated locations are where the data values have sharp gradients with few/no data points in the area. In Data Set #1 the shock is computed at 5.26. This is immediately after the sharp decrease around 5.0. The method computes 5.26 to be a shock rather than at 5.0 because of the number of data points along each gradient. The gradient at 5.0 has 13 data points along it, while the shock at 5.26 has only two. Again in Data Set #2, the shock at .21 has only two data points along it and the shock at 5.0 also has two. Both Data Set #3 and #4 have 3 data points at the shock, but this is to be expected because of the great jump in the function.

Periodic Data Results	
Data Set	Shock Location
Data Set #1	5.26921
Data Set #2	0.21559
	4.99108
Data Set #3	5.04608
Data Set #4	5.04558

Table 6.1: Computed shock locations from Physical Data.

6.2. 2–D Chebyshev Data. This data is the output of a numerical simulation run by Wai Sun Don (see figure 6.2). The simulation is of a shock wave interacting with a hydrogen bubble to produce combustion in a Hyper-sonic Jet. The numerical code was a 2–D Spectral code using Chebyshev polynomial in both directions.

The application of the Band Pass Filter Shock Location Technique was applied once in the x-direction and then once in the y-direction. The reason for applying the method is both directions is to ensure that shocks that are close to parallel with the x-direction are unlikely to be detected using a shock location technique in the x-direction. Applying this technique in both x and y directions will easily detected all shocks regardless of direction.

Figure 6.3 shows both the x and y computations. The computation contains a large shock front which was easily detected. The method also detects the hydrogen bubbles and the hydrogen spike. The hydrogen spike is an interesting feature of this computation. The spike occurs for a short time after the original single bubble breaks into two parts. This results in a very small area which contains mostly hydrogen. The difficulty is in detecting this hydrogen spike since it is really two shocks of opposite strength at almost the same location. This method does not correctly identify that there are two shocks here, but always finds one of the two shocks.

Another feature shown is the wake of the interaction for $x \in [.04, .06]$ which is clearly detected. Also detected are many very small shocks. Consider the shocks detected at $x = .120$. The flow has not reached this area yet, but there are small oscillations which have propagated ahead of the shock to $x = .120$. The shock computations are in the y-direction, so the function is very small overall. So these small oscillations seem larger and a shock is detected in the y-direction. Comparing the size of these shocks to the size of the major shocks shows that they can be ignored.

7. Comparisons and Conclusion . The Cell Shock Location part of this work provides two bits of information, number of shocks present and a first estimate of the shock locations. The first estimate is useful by itself. Gottlieb et al. have developed methods for reconstruction of discontinuous functions from the Fourier Coefficients using Gegenbauer Polynomials [8]. For this a estimate of each shock location is needed within Δx. This information from the Cell Shock Location can also be used in conjunction with Eckhoff's shock location technique [5] [6]. Eckhoff's work depends on knowledge of how many shocks there are. Using the band pass filtering method will determine the number of shocks present and then the Cell Shock Location will provide initial estimates to solve the system of equations in Eckhoff method.

The first part of this is consistent with some wavelet shock location techniques. Mallat and Zhong have done extensive work into finding many different kinds of edges using a continuous wavelet transform [15]. Wavelet techniques use filtering similar to this band pass filter shock location technique. Both rely on similarities of different filtered functions. The difference is in the application of the Sub–Cell filters.

The Sub–Cell Shock Location filter is a powerful tool. They are nearly compact, like wavelets, but these filters are designed to easily indicate the shock location. Wavelet edge detection depends on similarities between resolutions, but it is hard to find the shock location better than the finest scale. But the Sub–Cell filters designed provide a method which computationally are at least 3^{rd} order. Unlike Eckhoff's method, the Sub–Cell Filters maintain accuracy despite contact discontinuities.

Comparisons of the two methods were run on equations (5.27) and (5.28) and the results are displayed in tables 7.1 and 7.2. Table 7.1 shows that the Local Filter have similar errors as Eckhoff's Method using $Q = 2$. The results from using a Global Filter and Eckhoff's Method with $Q = 0$ (Prony Method) are also included. Q is a parameter for Eckhoff's algorithm.

Eckhoff's Method and Local & Global Filters (I)				
No Contact Discontinuity $f_a(x)$ [*eqn. 5.27*]				
	Sub-Cell Filters		Eckhoff's Method	
Points	Local Filter	Global Filter	Q = 0	Q = 2
64	7.12×10^{-3}	2.81×10^{-3}	4.2×10^{-3}	1.6×10^{-5}
128	8.40×10^{-7}	1.69×10^{-4}	7.6×10^{-4}	5.9×10^{-7}
256	3.01×10^{-8}	5.80×10^{-6}	1.6×10^{-4}	2.9×10^{-8}
512	1.01×10^{-9}	6.90×10^{-7}	4.0×10^{-5}	3.1×10^{-9}

Table 7.1: Comparison between Eckhoff's Method and the Sub–Cell Filters.

Table 7.2 shows the results of trying to locate the same four shocks but when there is a contact discontinuity in the data. The Global Filter maintains its accuracy, while the Local Filter looses some of its accuracy. If Eckhoff's method is applied searching for just the number of shocks in the function and there is a contact discontinuity, the method does not return a solution. However it was found that searching for the shocks and contact discontinuities will lead to accurate estimates. For example in table 7.2 the test functions have four discontinuities in the function and one discontinuity in the first derivative. Searching for only four shocks leads to bad estimates. Searching for five shocks leads to pretty good shock location estimates. The puzzling part of this is that searching for six shocks gives very good estimates. The solutions stay accurate for seven and eight shocks, but each time the system of equations becomes larger, and the solution takes longer to compute.

Eckhoff's Method and Local & Global Filters (II)					
Contact Discontinuity $f_b(x)$ [*eqn. 5.28*]					
	Sub-Cell Filters		Eckhoff's Method (Q = 2)		
Points	Local Filter	Global Filter	4 Shocks	5 Shocks	6 Shocks
64	1.94×10^{-2}	2.82×10^{-3}	N/A	N/A	1.67×10^{-2}
128	2.08×10^{-3}	1.65×10^{-4}	N/A	2.41×10^{-2}	1.45×10^{-6}
256	1.66×10^{-3}	5.80×10^{-6}	N/A	6.73×10^{-4}	4.66×10^{-8}
512	6.67×10^{-4}	6.93×10^{-7}	N/A	8.59×10^{-5}	1.98×10^{-9}

Table 7.2: Comparisons of problem with a contact discontinuity.

Overall, the band pass filter technique provides a quick method to find any number of shocks in the data as long as they are a minimum distance apart. Fortunately as the number of points increases the minimum distance which shocks need to be separated decreases. The Local Filter provides a better estimate to the shock locations, but at a cost. The method requires more computations and the error will increase if there are contact discontinuities. The Global Filter provides the quicker method to locate shocks and is not susceptible to have an increase in the error if the data contains a contact discontinuity. Global filters are best if the band pass filter technique needs to be applied many times.

8. Remarks. There are obvious extensions to this work. The first is that there exist filters, which evaluated at the shock location, give good estimations of the shock amplitude and the amplitudes of the jumps in other derivatives. For example, instead of using an even filter, use an odd filter. Then for a single shock at $x = 0$,

$$f_N^\nu(0) = A\, a_N^\nu(0). \tag{8.1}$$

$a_N^\nu(0)$ will be know, therefore

$$A\ \frac{a_N^\nu(0)}{f_N^\nu(0)} \tag{8.2}$$

Second, filters can be found to locate contact discontinuities once the shocks have been found. And more filters can be found to find spikes in the data.

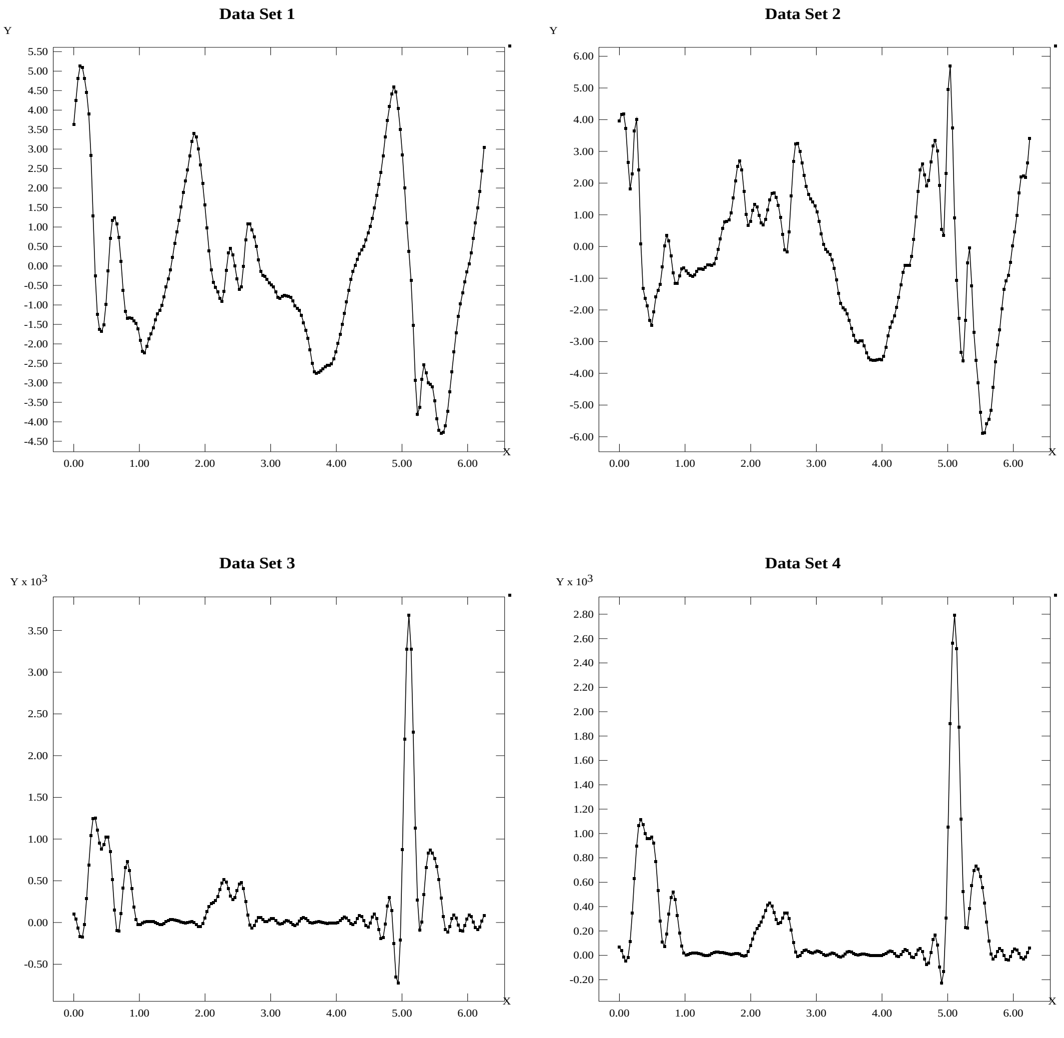

Fig. 6.1: 1–D Periodic Data: (*clockwise from top left*) Data Set #1 [observed wind], Data Set #2 [computed wind], Data Set #3 [elevation: un–filtered], Data Set #4 [elevation: filtered]

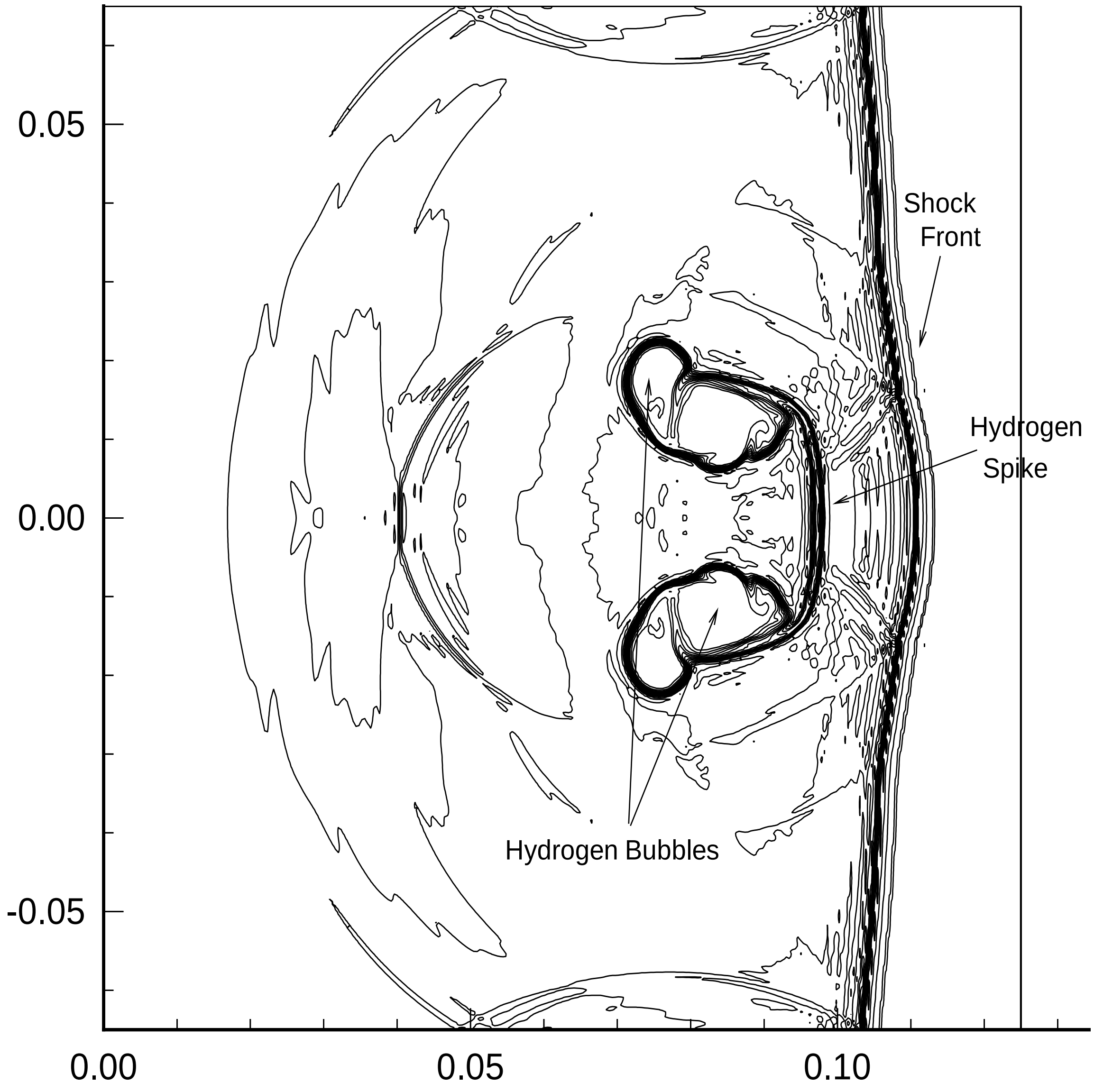

Fig. 6.2: Density of O_2 for Hydrogen Jet Computation. Figure 6.3 shows the locations of the different shocks shown in the contour plot. The important feature are the moving shock front, the hydrogen spike, and the deformed hydrogen bubbles.

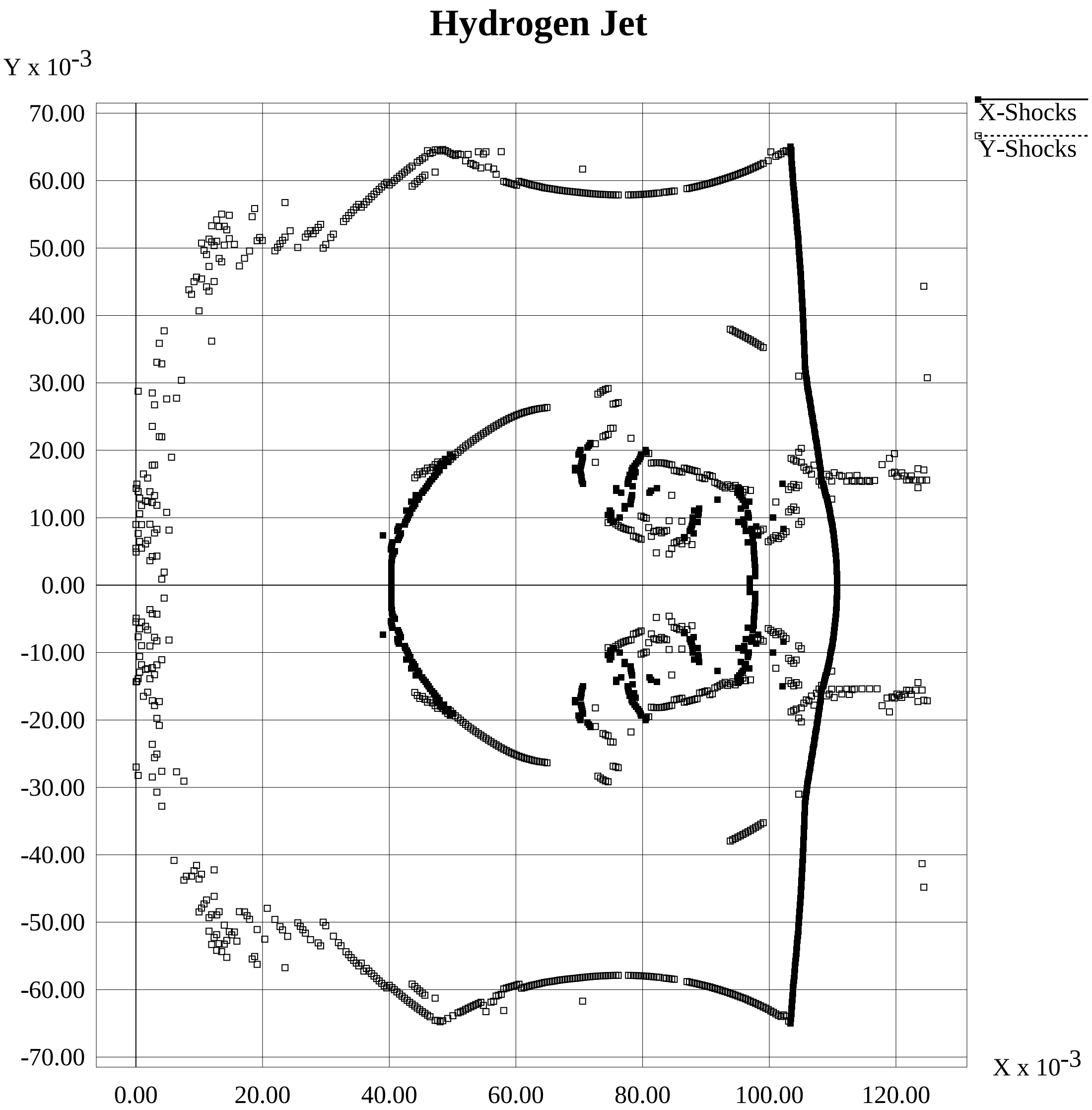

Fig. 6.3: Jet Shock Locations. The shocks found in the y-direction for $x < .3$ and in front of the shock front are numerical artifacts.

Appendix A. Wavelet Definitions . A discussion of wavelets is left to the appendix because wavelets only constitute a set of filters which can be used in place of the exponential and cosine filters described in section 1.4. Many more details of wavelets can be found in [11, 10, 3, 17].

A.1. Multi–resolution Analysis. Given a function $\phi(x) \in L^2(\mathcal{R})$. Define the dilation and translation of ϕ as

$$\phi_n^m(x) = 2^{-m/2}\, \phi(2^{-m}x - n). \tag{A.1}$$

The function ϕ is called the scaling function. Let V_m be the span of the functions ϕ_n^m.

$$V_m = \overline{\mathrm{span}\{\phi_n^m(x),\ \text{for } m, n \in \mathcal{R}\}}. \tag{A.2}$$

Definition A.1. *A multi-resolution analysis consists of a family of closed subspaces $V_m \in L^2(\mathcal{R})$, for $m \in \mathcal{R}$, such that*

(i)

$$\cdots \subset V_2 \subset V_1 \subset V_0 \subset V_{-1} \subset V_{-2} \cdots \tag{A.3}$$

(ii)

$$\bigcap_{m\in\mathcal{R}} V_m = \{0\} \qquad \overline{\bigcup_{m\in\mathcal{R}} V_m} = L^2(\mathcal{R}) \tag{A.4}$$

(iii) If $f(x) \in V_m$, then $f(2x) \in V_{m-1}$.

(iv) If $f(x) \in V_m$, then $f(x - 2^m n) \in V_m$, for $n \in \mathcal{R}$.

Let $\mathcal{P}_m$ denote the orthogonal projection onto V_m. Now examine the difference between $\mathcal{P}_m f$ and $\mathcal{P}_{m+1} f$. For multi-resolution analysis, define W_m as the orthogonal complement of V_m in V_{m-1},

$$V_{m-1} = V_m \bigoplus W_m, \qquad W_m \perp V_m. \tag{A.5}$$

It follows that

$$L^2(\mathcal{R}) = \bigoplus_{m\in\mathcal{R}} W_m, \tag{A.6}$$

and

$$L^2(\mathcal{R}) = V_M \bigoplus_{m\geq M\in\mathcal{R}} W_m, \tag{A.7}$$

A function $\psi(x)$ can be found such that its integer translates span W_0. The functions ϕ and ψ are the associated scaling function and wavelet function for the multi-resolution analysis spaces V_m and W_m.

A.2. Dilation Equation. Since $\phi \in V_0 \subset V_{-1}$, there exist c_n such that

$$\phi(x) = \sum_n c_n \phi(2x - n), \tag{A.8}$$

and since $\psi \in W_0 \subset V_{-1}$, there exist d_n such that

$$\psi(x) = \sum_n d_n \phi(2x - n). \tag{A.9}$$

where $d_n = (-1)^n \, c_{1-n}$. [3] These two equations are the dilation equations.

A.3. Orthogonality. Once scaling and wavelet functions have been defined, the basis functions are defined as the dilation and the translation of the scaling and wavelet functions.

$$\phi_n^m(x) = 2^{-m/2} \, \phi(2^{-m} \, x - n) \tag{A.10}$$

$$\psi_n^m(x) = 2^{-m/2} \, \psi(2^{-m} \, x - n) \tag{A.11}$$

For these functions to be an efficient set of basis functions, the sets of functions need to be orthogonal to each other.

$$\int \phi_k^j(x) \, phi_n^j(x) \, dx = \delta_{kn} \tag{A.12}$$

$$\int \phi_k^j(x) \, psi_n^j(x) \, dx = 0 \tag{A.13}$$

$$\int \psi_k^j(x) \, psi_n^j(x) \, dx = \delta_{kn} \tag{A.14}$$

A.4. Accuracy. Beyond orthogonality, the wavelets need to be able to accurately estimate functions. Wavelets are designed such that the first q moments of the wavelet are equal to zero.

$$\int x^p \, \psi(x) \, dx = 0 \qquad \text{for } p = 0, \ldots, q \tag{A.15}$$

A.5. Daubechies' Wavelets. Daubechies found coefficients c_n and d_n which satisfy definition A.1 and are compact in space. She was able to produce wavelets with the first $N/2$ moments equal to zero using only N non-zero coefficients. Table A.5 show the first three sets of coefficients she found.

Daubechies' Wavelet Coefficients, c_n

N	Coefficients
2	1,1
4	$(1+\sqrt{3})/(4\sqrt{2})$, $(3+\sqrt{3})/(4\sqrt{2})$, $(3-\sqrt{3})/(4\sqrt{2})$, $(1-\sqrt{3})/(4\sqrt{2})$
6	.3326705 . . ., .8068915 . . ., .4598775 . . ., −.1230110 . . ., −.0854412 . . ., .0352262 . . .

Table A.1: Daubechies wavelet coefficients for D_2, D_4, and D_6. N is the number of non-zero coefficients

A.6. Fourier Transform of Wavelet. From above, $\phi(x) = \sum_n c_n\,\phi(2x-n)$, multiply by $e^{-\imath\omega x}$ and integrate

$$\int \phi(x)e^{-\imath\omega x}\,dx = \int \sum_n c_n\,\phi(2x-n)e^{-\imath\omega x}\,dx \tag{A.16a}$$

$$= \sum_n c_n \int \phi(2x-n)e^{-\imath\omega x}\,dx \tag{A.16b}$$

$$= \sum_n c_n \frac{1}{2}\int \phi(x)e^{-\imath\omega(x+n)/2}\,dx \tag{A.16c}$$

$$= \sum_n c_n e^{-\imath\omega n/2}\frac{1}{2}\int \phi(x)e^{-\imath\omega x/2}\,dx \tag{A.16d}$$

Therefore

$$\widehat{\phi}(\omega) = \left\{\frac{1}{2}\sum_n c_n\, e^{-\imath\omega n/2}\right\}\widehat{\phi}(\omega/2) \tag{A.17}$$

Define

$$P(\omega) = \frac{1}{2}\sum_n c_n\, e^{-\imath\omega n} \tag{A.18}$$

then

$$\widehat{\phi}(\omega) = \prod_{j=1}^{\infty} P(2^{-j}\omega)\,\widehat{\phi}(0) \tag{A.19}$$

It follows directly that

$$\widehat{\psi}(\omega) = \frac{1}{2}\left(\sum_n d_n\, e^{-\imath\omega n/2}\right)\prod_{j=2}^{\infty} P(2^{-j}\omega)\,\widehat{\phi}(0) \tag{A.20}$$

Both $\widehat{\phi}(\omega)$ and $\widehat{\psi}(\omega)$ in equations (A.19) and (A.20) are well defined (see [3]). Since $\phi(x)$ is normalized to one, $\widehat{\phi}(0) = 0$.

EXAMPLE A.1. *Haar Wavelet*

The Haar Wavelet is the simplest wavelet and therefore the easiest to demonstrate wavelet properties, $c_0 = 1 = c_1$. *The scaling function is the box function*

$$\phi(x) = \begin{cases} 1 & \text{if } x \in [0,1] \\ 0 & \text{if } x \notin [0,1] \end{cases} \tag{A.21}$$

The wavelet is

$$\psi(x) = \begin{cases} 1 & \text{if } x \in [0,.5] \\ -1 & \text{if } x \in [.5,1] \\ 0 & \text{if } x \notin [0,1] \end{cases} \tag{A.22}$$

Using

$$P(\omega) = \frac{1+e^{-\imath\omega}}{2} \tag{A.23}$$

and (A.19)

$$\widehat{\phi}(\omega) = \frac{1}{4}(1+e^{-\imath\omega/2})(1+e^{-\imath\omega/4})\widehat{\phi}(\omega/4) \tag{A.24a}$$

$$= \frac{1}{4}(1+e^{-\imath\omega/2})(1+e^{-\imath\omega/4})\left\{\frac{1-e^{-\imath\omega/4}}{1-e^{-\imath\omega/4}}\right\}\widehat{\phi}(\omega/4) \tag{A.24b}$$

$$= \frac{1}{4}\left\{\frac{(1+e^{-\imath\omega/2})(1-e^{-\imath\omega/2})}{1-e^{-\imath\omega/4}}\right\}\widehat{\phi}(\omega/4) \tag{A.24c}$$

$$= \frac{1}{4}\left\{\frac{1-e^{-\imath\omega}}{1-e^{-\imath\omega/4}}\right\}\widehat{\phi}(\omega/4) \tag{A.24d}$$

(A.24e)

Applying equation (A.24d) multiple times and using

$$\lim_{p\to\infty}\frac{1}{2^p(1-e^{-\imath\omega/2^p})} = \frac{1}{\imath\omega} \tag{A.25}$$

results in

$$\widehat{\phi}(\omega) = \frac{1-e^{-\imath\omega}}{\imath\omega} \tag{A.26}$$

which is the same result as if the Fourier transform of phi(x) had been performed. The function $\widehat{\phi}(\omega)$ *is a low pass filter, but unlike the filters,* $\widehat{\phi}(\omega)$ *has an imaginary part. The function* $\widehat{\psi}(\omega)$ *is a high pass filter.*

$$\widehat{\psi}(\omega) = \frac{(1-e^{-\imath\omega/2})^2}{\imath\omega} \tag{A.27}$$

In the example above and for all scaling and wavelet functions, the two functions $\widehat{\phi}(\omega)$ and $\widehat{\psi}(\omega)$ make up a pair of filters, one low pass the other high pass.

Appendix B. Wavelet Expansion.

Now that the basis functions have been defined, it is possible to define the *wavelet expansion* of a function $f(x) \in L^2(\mathcal{R})$. Define the coefficients α_j and $\beta_{j,k}$ as

$$\alpha_{m,n} = \int f(x)\,\phi_n^m(x)\,dx \tag{B.1}$$

$$\beta_{m,n} = \int f(x)\,\psi_n^m(x)\,dx \tag{B.2}$$

Then

$$f(x) = \sum_m\sum_n \beta_{m,n}\,\psi_n^m(x). \tag{B.3}$$

This infinite summation is not possible for implementation on a computer. Therefore consider the sub-space V_M,

$$V_M = W_1 \oplus W_2 \oplus W_3 \ldots W_M \oplus V_M \tag{B.4}$$

Then consider the projection P_{V_M} of the function onto the space V_M as

$$f(x) = \sum_n \alpha_{J,n} \phi_n^J(x) + \sum_{m=1}^{M} \sum_n \beta_{m,n}\, \psi_n^m(x). \tag{B.5}$$

The result of this projection is that the lowest frequencies are captured by $\alpha_{J,n}$, and the higher frequencies are captured by $\beta_{m,n}$. Higher frequencies are captured by the coefficients with a higher m.

This is an important point for both appendixes. In finding shock locations these coefficients $\beta_{m,n}$ will be large around shocks. Therefore searching for large $\beta_{m,n}$ gives an estimate of the shock location. For the adaptive grid algorithm by Lee Jameson, high wavelet coefficients point out areas where addition resolution is required [9].

REFERENCES

[1] H. ANTON, *Elementary Linear Algebra*, Wiley, 1984.

[2] H. BATEMAN, *Higher Transcendental Functions*, vol. I, McGraw-Hill, 1953.

[3] I. DAUBECHIES, *Orthonormal bases of compactly supported wavelets*, Communications on Pure and Applied Mathematics, XLI (1988), pp. 909–996.

[4] P. J. DAVIS AND P. RABINOWITZ, *Numerical Integration*, Blaisdell Publishing Company, 1967.

[5] K. S. ECKHOFF, *Accurate and efficient reconstruction of discontinuous functions from truncated series expansions*, 1991.

[6] ———, *Accurate reconstruction of finite regularity from from truncated fourier series expansions*, 1993.

[7] D. GOTTLIEB AND S. A. ORSZAG, *Numerical Analysis of Spectral Methods*, Society for Industrial and Applied Mathematics, 1977.

[8] D. GOTTLIEB, C. W. SHU, A. SOLOMONOFF, AND H. VANDEVEN, *On the Gibbs Phenomenon I: Recovering expoenential accuracy from the Fourier partial sum of a non-periodic analytic function*, 1988.

[9] L. JAMESON, *On the wavelet-optimized finite difference method*, ICASE Report, (1994). Submitted to Journal of Computation Physics.

[10] S. MALLAT, *A theory for multiresolution signal decomposition: The wavelet representation*, IEEE Trans. Pattern Anal. and Machine Intel., 11 (1989), pp. 674–693.

[11] ———, *Multiresolution approximations and wavelet orthonormal bases of* $l^2(r)$, Trans. Amer. Math. Soc., 315 (September 1989), pp. 69–87.

[12] D. MARR, *Vision*, W.H. Freeman and Company, 1982.

[13] G. PÓLYA AND G. SZEGÖ, *Aufgaben und Lehrsätze aus der Analysis*, vol. 1, Spinger-Verlag, 1964.

[14] A. ROSENFELD AND M. THURSTON, *Edge and curve detection for visual scene analysis*, IEEE Trans on Computers, C-20 (1971).

[15] M. B. RUSKAI, ed., *Wavelet Transform Maxima and Multiscale Edges*, Jones and Bartlett Puslishers, 1992, p. 67.

[16] G. E. SHILOV, *Linear Algebra*, Dover, 1977.

[17] G. STRANG, *Wavelets and dilation equations: A brief introduction*, SIAM Review, 31 (1989), pp. 614–627.

[18] H. VANDEVEN, *Family of spectral filters for discontinuous problems*, Journal of Scientific Computing, (1987). Centre de Mathematiques Appliques.

[19] A. WITKIN, *Scale space filtering*, Proc. Int Joint Conf. Artificial Intelligence, (1983).